Atmos. Chem. Phys. Discuss., doi:10.5194/acp-2015-1056, 2016
Manuscript under review for journal Atmos. Chem. Phys.
Published: 16 February 2016

Atmospheric Chemistry and Physics Discussions

Impact of climate change on the production and transport of sea salt aerosol on European seas

J. Soares[1], M. Sofiev[1], C.Geels[2], J.H.Christensen[2], C.Andersson[3], S. Tsyro[4], J.Langner[3]

[1] Finnish Meteorological Institute, Helsinki, Finland

[2] Department of Environmental Science, Aarhus University, Roskilde, Denmark

[3] Swedish Meteorological and Hydrological Institute, Norrköping, Sweden

[4] EMEP MSC-W, Norwegian Meteorological Institute, Oslo, Norway

Correspondence to: J. Soares (joana.soares@fmil.fi)

Abstract

The impact of climate change on sea salt aerosol production, dispersion, and fate over the Europe is studied using four offline regional chemistry transport models driven by the climate scenario SRES A1B over two periods: 1990-2009 and 2040-2059. The study is focused mainly on European seas: Baltic, Black, North and Mediterranean. The differences and similarities between predictions of the individual models on the impact on sea salt emission, concentration and deposition due to changes in wind gusts and seawater temperature are analysed. The results show that the major driver for the sea-salt flux changes will be the seawater temperature, as wind speed is projected to stay nearly the same. There are, however, substantial differences between the model predictions and their sensitivity to changing seawater temperature, which demonstrates substantial lack of current understanding of the sea-salt flux predictions. Although seawater salinity changes are not evaluated in this study, sensitivity of sea-salt aerosol production to salinity is similarly analysed, showing once more the differences between the different models. An assessment on the impact of SSA to the radiative balance is presented.

Atmos. Chem. Phys. Discuss., doi:10.5194/acp-2015-1056, 2016
Manuscript under review for journal Atmos. Chem. Phys.
Published: 16 February 2016

Atmospheric Chemistry and Physics Discussions

1 Introduction

The sea salt aerosol (SSA) affects the Earth radiation budget, atmospheric chemistry, cloud processes, and climate (O'Dowd et al., 1997; IPCC, 2013). Anthropogenic and natural aerosols have similar annual impacts on the global radiative balance, though being predominant in different locations (Textor et al., 2006). SSA dominates the particulate mass and it is the major contributor to aerosol optical depth (AOD) over the ocean (Quinn et al, 1998).

SSA originates from sea spray droplets resulting from waves breaking on the seawater surface, forming whitecaps that cause the entrainment of air into the water. The two main mechanisms responsible for sea spray formation are air bubble bursting during whitecap formation and decay, and direct tearing of droplets from the top of breaking waves. Therefore, the formation of primary SSA is mainly dependent on wind speed: the emission of SSA is generally considered to be proportional to surface winds cubed (Monahan et al., 1986), suggesting that small changes in surface winds can have a substantial impact on the emission of this natural aerosol. Further on, studies on the marine aerosol size distribution (e.g. Covert et al., 1998; Russell and Heintzenberg, 2000; Bates et al., 2002; Huebert et al., 2003) suggest that for high wind speeds the production of very coarse SSA (with particle diameter (Dp) > 20 mm) increases, contributing to a higher transfer of heat and water vapour from the ocean to the atmosphere (Andreas et al., 1995). These processes have a strong impact on the climate forcing. Other parameters influencing the formation of primary SSA have been identified, e.g., seawater temperature and salinity, atmospheric stability, and wave height and steepness (O'Dowd and Smith, 1993; Gong et al., 1997; Gong, 2003; Mårtensson et al., 2003; Lewis and Schwartz, 2004; O'Dowd and de Leeuw, 2007; Witek et al., 2007a, 2007b; Ovadnevaite et al., 2014). Laboratory studies by Mårtensson et al. (2003) and in situ measurements by Nilsson et al. (2007) show that for nano-sized particles, the aerosol number emission decrease with increasing seawater temperature, and for particles with Dp > 100 nm, the number SSA increase with increasing seawater temperature; reflecting different sea spray formation processes. Seawater salinity also affects the droplet formation, where formation of particles with Dp < 0.2 µm are not affected by salinity, but for larger Dp's, salinity impact is substantial: higher salinity contributes to higher production (Mårtensson et al., 2003). The SSA removal processes are scavenging by precipitation and dry deposition (including gravitational settling). SSA has an effect on secondary aerosols formed by gas-to-particulate conversion process such as condensation and nucleation (binary homogeneous and heterogeneous) (Twomey, 1997). SSA serves as a sink for condensable gases and smaller aerosol particles, and serves also as a medium for aqueous-phase reaction of

Atmos. Chem. Phys. Discuss., doi:10.5194/acp-2015-1056, 2016
Manuscript under review for journal Atmos. Chem. Phys.
Published: 16 February 2016

Atmospheric Chemistry and Physics Discussions

reactive gases, e.g. H_2SO_4. This can lead to nucleation suppression for other components of the marine aerosol and consequently change their size distribution, creating a feedback on climate. Furthermore, SSA formation results in a size spectrum ranging from 0.01 to 100 µm, which can lead to cloud formation. With increasing concentrations of cloud condensation nuclei, the cloud microphysical properties change, i.e., the available water vapour is re-distributed over more particles, on average resulting in smaller particle sizes, which in turn changes both cloud albedo and precipitation (Latham et al., 2008, Lenton and Vaughan, 2009; Boyd, 2008; Korhonen et al., 2010, Wang et al., 2011). With dry diameter lower than 1 µm, SSA can easily be transported for long distances in the atmosphere, serving as a cloud seed outside of heavily clouded regions. The cloud drop number concentration can be spatially different, depending on the wind speed, atmospheric transport and particle loss via dry and wet deposition (Korhonen et al., 2010).

Changes in atmospheric transport pathways, precipitation patterns, and sea ice cover influence transport, removal and distribution of SSA. The main features of the regional and global SSA distribution and the climate impact on SSA production due to these physical drivers have been discussed in studies such as Liao et al. (2006), Pierce and Adams (2006), Manders et al. (2010), Sofiev et al. (2011), Struthers et al. (2011), and Tsyro et al. (2011). The understanding of sea spray emissions has increased substantially but process-based estimates of the total mass and size distribution of emitted sea spray particles continue to have large uncertainties (de Leeuw et al., 2011). Chemical transport models (CTM) and general circulation models (GCM) estimates of sea salt burden may vary over 2 orders of magnitude (Textor et al., 2006) and climate models disagree about the balance of effects, ranging from little (Mahowald et al., 2006a) to a considerable sensitivity to climate change (Bellouin et al., 2011). The difference between the available estimations might be due to the wind speed predicted by the climate models, with little understanding of how wind speed may change over the ocean in a warmer climate (IPCC, 2013).

The main goals of the current study are to assess the sensitivity of the production, surface concentrations and removal of SSA to climate change. A multi-model approach using four state-of-the-art offline CTMs was taken to assess the uncertainty/robustness of model predictions over Europe. The sensitivity of simulated emission, concentration, and deposition of SSA to changes in climate was evaluated by comparing a past (1990-2009) and a future (2040-2049) period. This study is a follow-up to the climates studies of Langner et al. (2012) focusing on surface ozone and Simpson et al. (2014) focusing on nitrogen deposition.

Atmos. Chem. Phys. Discuss., doi:10.5194/acp-2015-1056, 2016
Manuscript under review for journal Atmos. Chem. Phys.
Published: 16 February 2016

Atmospheric Chemistry and Physics Discussions

2 Methods

This study uses the same modelling structure as in Langner et al. (2012) for ozone and in Simpson et al (2014) for nitrogen. We focus on the comparison of SSA simulations from three offline European-scale CTMs - EMEP MSC-W, MATCH and SILAM - and one offline hemispheric CTM, DEHM. The models were run through a past (1990-2009) and a future (2040-2059) climate scenarios and the results for the European seas (Baltic, North, Mediterranean, and Black Seas) were compared. The climate meteorology data from a GCM were used in a regional climate model (RCM) and the hemispheric model DEHM. The regional models where driven by the downscaled meteorology from the RCM and the boundary conditions from DEHM. The horizontal grid for DEHM is 150x150 km^2 and for the regional CTMs identical to the RCM (ca. 50×50 km^2).

Throughout the paper, the SSA mass refers to the total mass of dry particles. Since the observations measure sodium (Na^+) concentrations rather than total SSA mass, it is assumed that Na^+ mass fraction is ~30% (Seinfeld and Pandis, 2006). Particle sizes are also provided for dry conditions and, unless otherwise stated, the dry diameter D_p ranges up to 10 µm.

2.1 Climate meteorology

Results of the global ECHAM5/MPIOM GCM (Roeckner et al., 2006), driven by emissions from the SRES A1B scenario (Nakicenovic, 2000), were downscaled over Europe with the Rossby Centre Regional Climate model, version 3 (RCA3) (Samuelsson et al., 2011; Kjellstrom et al., 2011). The global ECHAM5/MPIOM model is defined in spectral grid T63, which at mid-latitudes corresponds to a horizontal resolution of ca. 140×210 km^2. The horizontal resolution of RCA3 was 0.44º×0.44º on a rotated latitude-longitude grid, and data were provided with 6-hourly resolution. The climate, as downscaled by RCA3, reflects the broad features simulated by the parent GCM, but from earlier studies with the current setup it is clear that the global ECHAM5/MPIOM model projects a slightly warmer and wetter climate over Europe than the regional model RCA3 (Langner et al., 2012; Simpson et al., 2014).

The wind speed is higher over the ocean and can be up to two times slower, in average, over the inner seas (Fig. 1, first panel on the left). Wind patterns are different between the Seas, with some areas over individual seas being more affected by wind gusts than others: e.g. in the Mediterranean, the wind speed is higher over the Levantine Sea than over other areas. For the wind speed, RCA3 predicts an stronger increase at the Norwegian Sea, Black Sea, Gulf of Bothnia (Baltic Sea) and Aegean Sea (Mediterranean Sea) and a stronger decrease between Italy and Tunisia and Libya

Atmos. Chem. Phys. Discuss., doi:10.5194/acp-2015-1056, 2016
Manuscript under review for journal Atmos. Chem. Phys.
Published: 16 February 2016

Atmospheric Chemistry and Physics Discussions

(Mediterranean Sea) in the future period (Fig. 1, first panel on the right). Nevertheless, the absolute change is no more than 0.4 m/s. Trend analysis considering only marine grid cells for each sea (Fig. S1 in supplementary material) shows that there is no significant trend between past and future periods.

Typically, the surface water temperature is higher at southern latitudes. For the same latitude, the Black and Mediterranean Seas have, in general, higher temperature than the Atlantic Ocean and the Baltic Sea (Fig. 1, second panel on the left). RCA3 predicts a general increase of the water surface temperature between the past and the future periods (Fig. 1, second panel on the left). The most substantial changes are for the northern part of the Atlantic Ocean and for the Baltic Sea (maximum 1.17 ºC). Trend analysis for the monthly mean temperature is significant for all the European inner-seas (Fig. S2 in supplementary material). The temperature is rising for all the seas with the highest rise over the Black Sea and the lowest over the North Sea.

The precipitation tends to be higher over the ocean and lower over the inner seas. The lowest precipitation amount is seen over the Mediterranean Sea; on an annual level the difference from the ocean can be up-to two orders of magnitude (Fig. 1, third panel on the left). The climate model predicts that the precipitation will strongly decrease over the Mediterranean and increase over the Baltic and North Seas, whereas over different parts of Atlantic Ocean the opposite trends can coexist (Fig. 1, third panel on the right). Trend analysis shows that none of the trends is significant (Fig. S3 in supplementary material).

2.2 SSA boundary conditions

Sea salt concentrations (as fine and coarse modes, see the description of DEHM below) provided by the hemispheric DEHM model, were used as lateral and top boundaries for the regional models. The boundary values taken from DEHM were updated every 6 h and interpolated from the DEHM grid to the respective geometry of each regional CTM. The DEHM model was driven by the global ECHAM5-r3 meteorology, without the RCA-3 downscaling.

2.3 Chemical transport models

The models used in this study have been introduced in the previous studies: Langner et al. (2012) and Simpson et al. (2014). Below, we focus on their handling of the production and removal of SSA. All the SSA source functions in the current study are based on white-cap-area based parameterizations of Monahan et al. (1986), for formation of super-micron particles and follow

Atmos. Chem. Phys. Discuss., doi:10.5194/acp-2015-1056, 2016
Manuscript under review for journal Atmos. Chem. Phys.
Published: 16 February 2016

Atmospheric Chemistry and Physics Discussions

Mårtensson et al. (2003) for the sub-micron aerosols. The difference between the various source functions is the dependence on temperature and salinity for the SSA generation (**Table 1**).

2.3.1 DEHM

In DEHM the production of SSA at the ocean surface is based on two parameterization schemes describing the bubble-mediated sea spray production of smaller and larger aerosols. In each time step the production is calculated for seven size bins and thereafter summed up to give an aggregated production of fine (with dry diameters <1.3 µm) and coarse (with dry diameters ranging 1.3-6 µm) aerosols. For the fraction with dry diameters less than 1.25 µm a source function based on Mårtensson et al. (2003) is used, while for sizes larger than that the Monahan et al. (1986) source function is applied. They both include an $U_{10}^{3.41}$ dependency on wind speed and the production of the smaller aerosols is also a function of the sea surface temperature. An ambient relative humidity of 80% is assumed in the calculations and the size of the produced SSA is assumed to depend on the salinity at the actual location. Here a monthly climatology of current day salinity on a 0.25°x0.25° grid (Boyer et al., 2005) is applied for both time periods in focus in the current paper. Within the atmosphere, the fine and coarse fraction of SSA is treated separately in terms of transport and removal. Wet deposition includes in-cloud and below-cloud scavenging, while dry deposition velocities are based on typical resistance methods for various land surface types (see Simpson et al., 2003; Emberson et al., 2000). The fine and coarse fractions in the DEHM model are in the current paper assigned the dry diameters of 1 µm and 6 µm.

DEHM is continuously validated against available measurements from e.g. the EMEP network and an evaluation of an earlier version of the sea salt routine in DEHM showed that the model gives satisfactory results for sea salt over Europe (Brandt et al. 2012).

2.3.2 EMEP MSC-W

The standard Unified EMEP model runs include sea salt particles with ambient diameters up to about 10 µm, which mainly originate from the bubble mediated sea spray (Tsyro et al, 2011). The parameterisation scheme for calculating sea salt generation in the EMEP model makes use of two source functions for bubble-mediated sea spray production. The first one is a source function for sea spray droplets at 80% relative humidity from Monahan et al. (1986) and the second one is a source function for sea salt particles from the work of Mårtensson et al. (2003), which is formulated for a salinity of 33‰. In the EMEP model, the SSA fluxes can be calculated for particle dry Dp ranging from 0.02 to 12 µm, whereas operationally and for this work SSA with Dp up to 6 µm are included.

Atmos. Chem. Phys. Discuss., doi:10.5194/acp-2015-1056, 2016
Manuscript under review for journal Atmos. Chem. Phys.
Published: 16 February 2016

Mårtensson et al. (2003) parameterisation is applied for smaller size bins, while Monahan et al. (1986) parameterisation is used for the coarser ones. From the fluxes of sea spray, the sea salt mass is calculated assuming sea salt density of 2200 kg/m3. The total production rates of fine and coarse sea salt are calculated by integrating the size resolved fluxes (7 in the fine and 3 in the coarse fractions) over respective size intervals. In the model, generated SSA is assumed to be instantaneously mixed within the model lowest layer at each time step. The transport and removal of sea salt is described individually for the fine and coarse fractions in the EMEP model. Dry deposition parameterisation for aerosols is calculated using a mass-conservative equation from Venkatram and Pleim (1999). The dry deposition due to gravitational settling is size-dependent and diameters of 0.33 and 4.8 μm are assumed for the fine and coarse SSA. . Wet scavenging is treated with simple scavenging ratios, accounting for in-cloud and sub-cloud processes. The scavenging ratios are assigned to crudely reflect the solubility of different aerosol components, and the size differentiated collection efficiencies are used in sub-cloud aerosol washout.

The present sea salt parameterisation was shown to give the best overall results as compared to a number of other source functions within the EMEP model (Tsyro et al., 2011). The model SSA calculations are extensively evaluated against long-term observations (Tsyro et al., 2011; EMEP Reports http://www.emep.int).

2.3.3 MATCH

The treatment of SSA production in MATCH is based on the parameterization of Mårtensson et al. (2003) for dry particle sizes of up to 0.4 μm aerodynamic radius, and on Monahan et al. (1986) for larger particle sizes. The temperature correction following Sofiev et al. (2011) is applied to the estimates from the Monahan scheme. The number of bins is flexible, but in this study four size bins were used with Dp ranges 0.02–0.1 μm, 0.1–1 μm, 1–2.5 μm, 2.5–10 μm. The production of sea salt droplets is calculated assuming an ambient relative humidity of 80% and a particle density of 1150 kg/m3 and is integrated over each size bin while dry removal rates are calculated using the geometric mean size in each bin. Dry deposition over land is following Zhang et al. (2001) while a separate parameterization accounting for bubble burst activity is used over sea (Pryor and Barthelmie, 2000). Sea salt is assumed to 100% activated or scavenged by hydrometeors in-cloud while below-cloud scavenging is handled following Dana and Hales (1976). The distribution of salinity in sea water is taken from NOAA (2013). Further details and evaluation of MATCH sea salt simulations using observed meteorology can be found in Foltescu et al. (2005) and Andersson et al. (2014).

Atmos. Chem. Phys. Discuss., doi:10.5194/acp-2015-1056, 2016
Manuscript under review for journal Atmos. Chem. Phys.
Published: 16 February 2016

Atmospheric Chemistry and Physics Discussions

2.3.4 SILAM

The SSA production via bubble-mediated mechanism takes into account the effects of wind speed, salinity, and water temperature and covers sea salt particles with dry diameter from 20 nm to 10 µm. The observations from the Mårtensson et al. (2003) study for seawater surface temperature 298 K and sea water salinity 33 ‰ were used to extrapolate the scheme from Monahan et al. (1986) to particle sizes down to 20 nm. To calculate SSA production for other water temperatures and salinities, correction factors are applied which were derived based on the experimental data of Mårtensson et al. (2003). The full description of the parameterisation in the SILAM model can be found in Sofiev et al. (2011). The description of the temperature correction in Sofiev et al. (2011) was changed. Currently, the water temperature reference for the unified shape function is 20 ºC, instead of 25 ºC as referred in Sofiev et al. (2011). The shape function has been updated accordingly and the new shape function (dF_0/dD_p) for particles with Dp ranging from 0.01 to 10 µm is described below:

$$\frac{dF_0}{dD_p} = (1 + 0.05 * D_p) * \frac{\exp\left(\frac{-0.11}{D_p}\right)}{0.4 + \exp\left(\frac{-0.2}{D_p}\right)} * \frac{6 * 10^5}{\left(1 * 10^{-4} * D_p^2 + D_p\right)^3} * 10^{1.19 * \exp\left(-\left(\frac{0.35 - \lg D_p}{0.8}\right)^2\right)} \quad (1)$$

For the current study the spume droplet formation based on Andreas (1998) was included, with spume being supressed for 10m wind speed lower than 6 m/s. The production of sea salt droplets is calculated assuming a dry particle density of 2200 kg/m^3. The size distribution is described by flexible bins. Production is integrated over each size bin while dry and wet removal rates are calculated using mass-weighted mean diameter in each bin. Depending on particle size, mechanisms of dry deposition vary from primarily turbulent diffusion driven removal of fine aerosols to primarily gravitational settling of coarse particles (Kouznetsov and Sofiev, 2012). Wet deposition distinguishes between sub- and in-cloud scavenging by both rain and snow (Sofiev et al., 2006; Horn et al., 1987; Smith and Clark, 1989; Jylhä, 1991). Gravitational settling, dry deposition and optical properties take into account the particle hygroscopic growth. For the simulations, five bins with the Dp ranges of 0.01–0.1 µm, 0.1–1.5 µm, 1.5–6 µm, 6–15 µm; and 15-30 µm were used. The distribution of salinity in sea water is taken from NOAA (2013).

SILAM model has been evaluated against a wide range of observations and models utilizing the above described parameterization (Sofiev et al., 2011; Tsyro et al., 2011).

Atmos. Chem. Phys. Discuss., doi:10.5194/acp-2015-1056, 2016
Manuscript under review for journal Atmos. Chem. Phys.
Published: 16 February 2016

Atmospheric Chemistry and Physics Discussions

2.4 Model evaluation

Sea water is the predominant source of Na^+ in the atmosphere, which can be used as its tracer in most regions of Europe. Evaluation of the model predictions was performed via comparison with observations available from the EMEP network (Co-operative Programme for monitoring and evaluation of the long-range transmission of air pollutants in Europe, http://www.emep.int, Tørseth et al. 2012) that perform regular measurements across Europe. The observations include Na^+ concentration in aerosol and ion analysis of precipitation including Na^+. Concentration measurements are sampled daily by a filter pack sampler (cut-off at D_p = ~10 µm), at 2 m height; the concentration in precipitation is mainly sampled by a "wet-only" sampler and, in a few places, with bulk collectors. The wet deposition of Na^+ is obtained by multiplying the weighted mean concentration by the total amount of precipitation in a daily basis. For more details about the sampling the reader is referred to e.g., Hjellbrekke and Fjæra (2009). These sampling methods do not distinguish if the sodium is originated from natural (e.g. mineral dust) or anthropogenic sources. In some regions there might be certain amounts coming from combustion processes and industry, but overall the contribution of anthropogenic sources to the sodium budget is low (van Loon et al., 2005).

The measurement data were averaged to monthly level with the minimum completeness requirement of 75% temporal coverage per month and per year, between 1990 and 2009. The CTMs predictions for the measurement sites satisfying the temporal criterion were averaged on a monthly basis over the 20 years. Since the model computations were driven by climate model fields, no temporal collocation was done. Therefore, the primary parameter considered was the monthly Na^+ concentrations averaged over the past period. Modelled values were obtained from the model's lowest layer mid-point, which is defined somewhat differently for each model (**Table 1**). No near-surface concentration profiling was made, with the exception of EMEP where concentrations are corrected to 3 m height, largely due to unreliable stability estimates based on climate-model fields.

The model performance was evaluated by the following statistical measures: bias, spatial Pearson correlation coefficient (R), root mean square error (RMSE), bias and standard deviation (SD) ratio ($SD_{model}/SD_{observations}$). The evaluation included Na^+ concentration in aerosols at 29 measurement sites and ion analysis of Na^+ wet deposition at 133 measurement sites, which we consider sufficient for computing the basic statistical scores and plotting scatter plots. The location of the measurement sites are shown in Fig. S4 in the supplementary material.

Atmos. Chem. Phys. Discuss., doi:10.5194/acp-2015-1056, 2016
Manuscript under review for journal Atmos. Chem. Phys.
Published: 16 February 2016

Atmospheric Chemistry and Physics Discussions

2.5 Radiative transfer modelling

The radiative transfer modelling was completed offline with the libRadtran software package for radiative transfer calculations (Mayer and Kylling, 2005). This tool calculates radiances, irradiances and actinic fluxes for the given optical properties. The Earth radiative balance results from the difference between the incoming (direct and diffusive-downwards) and outgoing (diffusive upwards) radiation. The impact of SSA is assessed by the difference between an atmosphere with SSA and without SSA, for the past and future periods. The calculations were defined at the top of the atmosphere (TOA), with wavelength ranging from 0.2 to ~4 µm, in order to compute the integrated shortwave irradiance. All the runs considered wet and icy clouds, with the cloud cover taken from the climate model RCA3 and optical properties taken from MODIS observations (Pincus et al. 2011). Monthly-basis observations from AQUA and TERRA obtained from 2002 to 2014 were averaged in order to have climatological cloud optical fields. These fields were the same for both past and future period calculations. Earth albedo information is included in the calculations and is obtained from the NASA model, GLDAS Noah Land Surface Model L4 (Rodell et al., 2004), on a monthly basis for the period between 1990 and 2012. This dataset was averaged to obtain climatological surface albedo fields, remaining the same for both past and future periods. The calculations for an atmosphere with SSA included the AOD computed by SILAM: the AOD at 550 nm was computed for the full size-spectrum of the SSA described in Table 1. SILAM's optical thickness predictions are based on size distribution and spectral refractive index of SSA (Prank, 2008). The AOD data was monthly-averaged for every hour in a day, for the past and future periods. This allowed taking into consideration the length of the day, since solar zenith angle is computed for every hour. The description of the runs and assumptions are provided in Table 2. This setting was chosen in order to reflect an atmospheric state closer to reality, since there were no other aerosols available for this study. Keeping the atmospheric and cloud conditions constant between the past and the future, will allow pinpointing the impact of the SSA on the radiative balance.

3 Results

3.1 Comparison with observations

Figure 2 and Figure 3 show the performance of the CTMs estimating Na^+ surface concentrations and wet deposition, respectively, during the past period; Table 3 and Table 4 complete the statistical evaluation of the models for the surface concentrations and wet deposition, respectively. The

Atmos. Chem. Phys. Discuss., doi:10.5194/acp-2015-1056, 2016
Manuscript under review for journal Atmos. Chem. Phys.
Published: 16 February 2016

models showed similar performance with quite high correlation coefficients varying from 0.71 up to 0.85 for the concentrations but substantially lower for wet deposition (from 0.24 up to 0.41). The difference between the model performances is quite small and varying for the different scores. The highest correlation with the concentration observations was shown by DEHM (0.85), which also demonstrated the highest RMSE and bias originating from a stronger overestimation over the regions with observed low concentrations. EMEP showed the lowest RMSE and bias, as well as one of the best correlation factors. SILAM tends to overestimate the lowest observed values (positive bias) whereas MATCH has a stronger underestimation of the highest values (negative bias). Comparing the winter (December, January and February) and the summer (June, July and August) seasons, one can notice that the models perform better in summer, with higher correlation and lower bias. The observed winter time levels are likely harder to be reproduced due to stronger winds and faster changing weather, which might not be captured by the climatological runs.

Comparison of Na^+ wet deposition with measurements shows low correlation and substantial under-prediction. This is particularly true for the high-deposition observations, which resulted in a strong negative bias for all the models. The evaluation of modelled precipitation was presented in Simpson et al. (2014), Table 4, and shows an overestimation of precipitation in the RCA3 model (reginal CTMs) and underestimation in the precipitation used in DEHM. The overestimation leads to an overestimation of the deposition of SSA close to the sources. Consequently, less SSA reaches the shore and the measurement sites. The second major reason for discrepancy is that the observed wet deposition does not cut-off the size of the particles, i.e. SSA coarser than 10 µm is accounted for, including the SSA produced in the surf zone. This mostly explains the large negative bias of the models, which reported PM_{10} only, and, to some extent, the low correlation. This is demonstrated when comparing SILAM scores taking into account the full size range available (Dp = [0.01-30] µm): accounting for the coarser aerosols strongly reduced the bias, correlation strongly improved, and RMSE became slightly smaller. In summer, the scores are slightly better than in winter, but the absolute values and importance of this removal process is smaller in summer time.

In Simpson et al. (2014), it was shown that CTMs driven by RCM meteorology are likely to perform worse than they would with data from numerical weather prediction models. Nevertheless, the current comparison showed that CTMs can predict mean concentrations and depositions within ~30% uncertainty (for depositions, prediction of full size range is a pre-requisite), whereas the spatial distribution patterns are reproduced with correlation higher than 0.7 also when driven by climate model meteorology.

Atmos. Chem. Phys. Discuss., doi:10.5194/acp-2015-1056, 2016
Manuscript under review for journal Atmos. Chem. Phys.
Published: 16 February 2016

Atmospheric Chemistry and Physics Discussions

3.2 Current and future climate SSA emissions

The annual SSA emission in the reference period predicted by DEHM, MATCH and SILAM is shown in Figure 4 (left panel). EMEP did not have this variable as an output. As expected, all models predict the highest emissions over the Atlantic Ocean, with the Mediterranean Sea being the second highest source. MATCH predicted, in average, 25% higher emissions over the Mediterranean than SILAM. The emissions are mainly driven by the wind and typically expressed by the white-cap produced by the surface-winds via the Monahan and O'Muircheartaigh (1980) parameterisation. This empirical power-law is taken by all models participating in this study and suggests emission (E) to be proportional to the 10m-wind speed (U_{10}) to the power of 3.41: $E \approx U_{10}^{3.41}$, the so-called wind-forcing. Consequently, the SSA emissions (Fig. 4, left panel) clearly correlate with the wind-forcing (Figure 5, left panel), in particular over the open ocean. However, the use of the same functional dependence and input meteorology does not guarantee identical emission, as it will be discussed further on. MATCH and SILAM seem more sensitive to the wind-forcing over the Mediterranean than DEHM, possibly due to the horizontal resolution difference between the hemispheric and regional CTMs (e.g. the Mediterranean is not properly resolved by the global climate model, the driver for DEHM). Apart from the wind forcing, laboratory studies have shown the relation between the emissions of SSA and seawater surface temperature and salinity: SSA mass will be higher at sea areas with higher surface water temperatures and salinity (Mårtensson et al, 2003). The temperature and salinity dependencies are included in the parameterizations, therefore, the models predict for the same wind forcing, higher emissions for higher water temperatures: the Mediterranean and Black Seas (Fig. 1 and Fig. 4, left panel). The effect of salinity is best seen in the Baltic Sea (salinity ~ 9 ‰), which has comparable wind forcing to some areas of the Mediterranean and the Atlantic (salinity ~33 ‰) but lower emission. SILAM and MATCH show the highest difference between the inner-seas with at least 3 times lower emissions over the Baltic Sea.

In absolute terms, the climate impact on SSA emissions (Fig. 4, right panel) is mainly positive according to the regional models whereas DEHM shows a general decrease. The exception goes for the Atlantic Ocean, in the west side of the domain, where all the models agree in a decrease of emissions. The difference between the past and future periods is only due to the wind forcing and temperature changes, since salinity was kept constant. Thus, this change (Fig. 4, right panel) highly correlates with the changes for wind-forcing (Fig. 5, right panel), adjusted by the changes in water temperature (Fig. 1, right panel). For example, the pronounced decrease of emission over western

Atmos. Chem. Phys. Discuss., doi:10.5194/acp-2015-1056, 2016
Manuscript under review for journal Atmos. Chem. Phys.
Published: 16 February 2016

Atlantic is mainly driven by the reduction of wind speed but the decrease is limited by the rising temperature in the north and east: higher temperature leads to production of more SSA even for somewhat slower wind speed.

The models demonstrated different sensitivity to seawater temperature: it seems to be less important for DEHM than for other models, whereas SILAM is the most sensitive. For instance, MATCH and SILAM showed an increase of emissions over the east of Iceland where temperature is predicted to rise by almost 2 K. The increase of seawater temperature, supported by higher wind speed, over the Black and Aegean Seas (Fig. 1, right panel), will lead to higher emissions. DEHM might not be so sensitive to the local storms due to the coarse horizontal resolution. The absolute difference between future and past is the smallest for the Baltic Sea, but in relative terms all the models show an increase up to 20% in Gulf of Bothnia, which is actually higher than, e.g. 5-15% of increase predicted for North Sea (minimum for DEHM and maximum for MATCH).

Trend analysis for the Baltic, Black, Mediterranean and North Seas (only sea cells are taken into consideration) is available as supplementary material: Fig. S5 for the Baltic, Fig. S6 for the Black, Fig. S7 for the Mediterranean, and Fig. S8 for the North Seas. The trend is only statistically significant ($p < 0.001$) for all the models for the Black Sea, with all models agreeing on an increase of concentration in the future.

Figure 6 (left panel) shows the SSA emission difference between the winter and summer for the past period. The difference between seasons in terms of SSA production can be substantial: SSA emission is up to 3 times higher in winter time. Seasonally, there are differences between the driving processes for SSA production: the winter period has a larger SSA production, due to more frequent and stronger storms; but the summer time shows pronounced maxima over specific areas mostly influenced by the seawater temperature. The latter is mostly true for MATCH and SILAM, since their temperature sensitivity is higher. SSA emission in winter will be accentuated in the future for MATCH (more emphasized) and SILAM: Figure 6 (right panel) shows pronounced maxima around Iceland and the British Isles; distinct differences in the SSA emission are also seen in the Mediterranean. DEHM does not show much difference between the periods.

3.3 Current and future climate SSA concentrations

Concentration is a function of emission and transport of the SSA, that is dependent on ventilation of an area over inner seas (wind speed), and on removal processes largely controlled by precipitation and relative humidity (via settling). Generally, the pattern of SSA concentration follows the

Atmos. Chem. Phys. Discuss., doi:10.5194/acp-2015-1056, 2016
Manuscript under review for journal Atmos. Chem. Phys.
Published: 16 February 2016

emission areas with stronger winds and frequent storms. Concentrations are, therefore, higher at the Atlantic Ocean and lower at the European inner-seas. All the models show lower concentrations for the Baltic Sea, reaching up to 10 times difference from the ocean (Fig. 7, left panel). The Mediterranean Sea is the inner sea with the highest concentrations. For the Baltic Sea, DEHM and MATCH show the highest and the lowest concentrations, respectively, with a difference of a factor of ~1.3 between each other. For the Black Sea, DEHM and EMEP show the highest concentrations and a similar spatial distribution pattern, and SILAM the lowest; nonetheless the difference is not so substantial. For the Mediterranean Sea, EMEP shows the lowest concentrations, MATCH being the highest: with 30% difference. All models show pronounced maximums at the Balearic Sea and the Levantine Sea. Transport over land is quite similar among the models, especially for the regional CTMs. The biggest difference lies over the western-central Europe with MATCH showing lower concentration over land. Transport of SSA inland is visible hundreds of km's inland; near the coast line it can contribute up to 6 $\mu g/m^3$ to PM_{10}.

The models predict relatively similar pattern for the SSA spatial distribution for the past period but, they seem to have different responses to the future climate, with MATCH and SILAM clearly being the most sensitive and EMEP the least. Figure 7 (right panel) shows the difference between the past and future periods for the different models. DEHM and EMEP foresee almost no change or a decrease of SSA concentrations over the open sea, whereas MATCH and SILAM predict an increase. These results were expected due to the predicted emissions (Sect. 3.2). All models agree in an increase in SSA surface concentration over the north of Iceland, the Black Sea, and over land in southern latitudes. The models agree somehow on an increase of the Mediterranean and Black Seas SSA concentration but it is MATCH and SILAM that show the highest positive change in concentrations. The impact over land is slightly positive for all the models in the Southern part of the domain, while at more Northern latitudes DEHM and EMEP from one side, and MATCH and SILAM models from another, disagree on the trend signal: a reduction of the SSA load over land is predicted by the first two models and an increase by the latter pair.

Overall, EMEP is the least sensitive and MATCH the most sensitive model to a changing climate. SILAM is the most sensitive over the Norwegian Sea. The difference between the past and future period concentrations is more substantial than that of emissions: the factors seemingly having exacerbated this difference are the decrease of ventilation over the west-Mediterranean, changes in mixing patterns, etc.

Atmos. Chem. Phys. Discuss., doi:10.5194/acp-2015-1056, 2016
Manuscript under review for journal Atmos. Chem. Phys.
Published: 16 February 2016

Trend analysis (supplementary material: Fig. S9 for the Baltic, Fig. S10 for the Black, Fig. S11 for the Mediterranean, and Fig. S12 for the North Seas) suggest that trends are only significant ($p < 0.001$) for MATCH and SILAM for both Mediterranean and Black seas, all with a positive signal.

Seasonally, the concentrations follow the same pattern as the emissions: higher in winter time. When analysing the changes between winter and summer, the models can again be grouped into DEHM-EMEP and MATCH-SILAM. In winter (Fig. 8, left panel), the first pair presents a larger amount of SSA mass generally over sea and land surfaces. Conversely, MATCH and SILAM predict a decrease of SSA surface concentration around the British Isles, Mediterranean and Black Seas, though the coast lines have sharper peaks of SSA mass during winter. The difference between the future and past periods (Fig. 8, right panel) is relatively similar for all the models over the open sea: predictions show an increase of concentration around the British Isles and a decrease over the Norwegian Sea, in the future. MATCH and SILAM show sharper increase or decrease along the Mediterranean Sea. The changes predicted can be 3 times higher than the changes predicted for the emissions (Figure 6, right panel). The changes can also have different signal, e.g. the Eastern-basin of the Mediterranean where it is predicted an increase of emissions but a decrease of concentrations, implicating that the ventilation over this area was quite effective.

3.4 Current and future climate SSA deposition

The deposition (wet+dry) patterns for SSA are depicted in Fig. 9 (left panel). Typically the deposition is higher over the sources areas and close to the coastal areas. Over land, SILAM shows less deposition and DEHM and EMEP predict the highest levels. There are different patterns over the Atlantic, mostly attributable to the boundary conditions treatment by each model. DEHM predicts quite high values over all the seas. Over the Black Sea, the deposition is more accentuated in the predictions by EMEP and less by SILAM. MATCH also shows higher values for deposition over the Mediterranean, and SILAM the lowest. Deposition is not substantial over the Baltic Sea, with exception of DEHM, owing to low SSA mass released from its surface.

The impact of future climate conditions (Fig. 9, right panel) on deposition, in absolute levels, is small and mostly noticeable over the Atlantic Ocean. For all models, the most significant positive change in the deposition is seen around Iceland. This is expected according to the changes seen in precipitation between future and past periods (Fig. 1, third panel on the right). All regional CTMs show a strong signal on the west side of the domain, an artefact due to the boundary conditions. In

Atmos. Chem. Phys. Discuss., doi:10.5194/acp-2015-1056, 2016
Manuscript under review for journal Atmos. Chem. Phys.
Published: 16 February 2016

relative terms, Scandinavia, east of UK, central-western Europe and Mediterranean are the most affected with 5-20% more deposition predicted by MATCH and SILAM.

Trend analysis (supplementary material: Fig. S13 for the Baltic, Fig. S14 for the Black, Fig. S15 for the Mediterranean, and Fig. S16 for the North Seas) suggests that none of models show a significant trend.

Seasonally, SSA deposition is higher in winter than in summer, due to the higher emissions and frequent precipitation in winter months. This difference is mainly accentuated over the source areas: MATCH and SILAM have the lowest difference over the Baltic and Black Seas, due to the lower production; DEHM shows the highest at Mediterranean Sea. The difference of deposition between winter and summer will also change in the future period (Fig. 10, right panel) with all models showing a slight increase of the deposition in summer over the Mediterranean and along the coast of Norway. An increase of deposition in winter was suggested around Iceland and British Isles, North Sea and coastal areas of Mediterranean Sea.

4 Impact of meteorology and seawater properties on the emission and fate of SSA

The multi-model comparison presented in Sect. 3 shows that there are significant difference between the models in terms of emission and fate of the SSA. The latter is particularly true for the inner seas. The differences between the models lead to a more uncertain answer about the impact of the future climate on the production and transport of SSA and its possible feedback to climate. The SSA emission in the models is driven by three parameters: wind speed, water temperature, and water salinity. All models use the same $U_{10}^{3.41}$ dependence on wind speed; hence the differences in emission have to be attributed to parameterization of temperature and salinity dependencies. Formally, all models used the Monahan et al. (1986) and Mårtensson et al. (2003) parameterizations or, at least, the available data for deriving the emission flux parametrizations (SILAM). Specifics of the implementation, however, appeared significant. To understand the latter, box-model calculations of the SSA mass flux as a function of temperature were made for seawater salinity 10 and 35 ‰, representing Baltic Sea and Atlantic Ocean, respectively, and with wind-speed fixed at 15 m/s (Fig. 11, left-hand panel).

In general, all the models show an increase of mass flux of SSA with temperature and salinity, except EMEP that does not apply any correction for salinity. Both DEHM and EMEP mass flux show little difference between low and high temperatures; SILAM and MATCH show a substantial

Atmos. Chem. Phys. Discuss., doi:10.5194/acp-2015-1056, 2016
Manuscript under review for journal Atmos. Chem. Phys.
Published: 16 February 2016

dependency of the mass flux on temperature throughout the size ranges. This difference is explained by the way dependency on seawater temperature is implemented: only for the fine mode in DEHM and EMEP, based on the Mårtensson et al. (2003) source function, and for both fine and coarse modes in SILAM and MATCH. In MATCH, the implementation of seawater temperature correction is done by combining the temperature correction included in the Mårtensson et al. (2003) for size-range below Dp = 0.4 µm and the use of the temperature corrections from Sofiev et al. (2011) for the coarser sizes. In SILAM the source function is scaled with Sofiev et al. (2011) size-dependent temperature correction function. This explains why the results in Sect. 3 could be paired between the models. EMEP is the model that shows the highest amount of SSA produced, with the exception for seawater temperature higher than 15 ºC and high salinity, with MATCH and SILAM predicting the highest amount of SSA. For the lowest salinity, SILAM is the model that produces less SSA, with DEHM being surpassed by MATCH around 17 ºC. For the highest salinity, both MATCH and SILAM start to predict higher SSA flux than DEHM around 9 ºC. This is due to the temperature correction factor described in Sofiev et al. (2011) that assumes that for low seawater temperature, the production of coarse SSA, where the mass is significant, is very low. This analysis clarifies why MATCH and SILAM tend to have higher emissions than DEHM where waters are warmer and lower when colder (e.g. Baltic Sea), and why MATCH shows the highest values for the SSA mass flux. Also explains the smaller difference between winter and summer predicted by DEHM, since the changes in SSA mass flux depending on seawater temperature is very low.

Figure 11 (right panel) shows how the different models distribute the mass between the fine and coarse modes, for the same wind and salinity conditions described above. Both DEHM and EMEP assume that the contribution of the coarser mode is reduced with temperature, since more SSA is produced with higher temperatures, for size ranges below 2.5 µm. EMEP has the highest contribution for the coarse mode, independent of the temperature. For MATCH and SILAM, the contribution to the coarser mode increases with temperature, though MATCH has a lower coarse mode contribution than SILAM. The only agreement between the DEHM, MATCH and SILAM is that for higher salinities, the coarse mode contribution is higher. The ratio between fine and coarse mode is very relevant for the deposition processes, and it could explain why deposition is higher for DEHM and EMEP (Fig. 9), though in this case, it is hard to evaluate the real impact due to different deposition schemes implemented in the models.

It is pertinent to discuss the difference between DEHM, EMEP and MATCH, since these models apply the same parameterization for SSA number flux, though having different salinity fields and

Atmos. Chem. Phys. Discuss., doi:10.5194/acp-2015-1056, 2016
Manuscript under review for journal Atmos. Chem. Phys.
Published: 16 February 2016

salinity correction function. Mårtensson et al. (2003) defines very strict size ranges for the computation of the 6^{th} order polynomial for particles between 0.02 to 2.8 µm in dry diameter. In case the models define size ranges outside of the tabulated in that study, it can result in very different results. The linkage between the two parameterizations can also result in different outcomes: DEHM links the two parameterizations at dry diameter of 1.25 µm, EMEP at 1.5 µm and MATCH at 0.4 µm. In the case of MATCH, an extrapolation of the Monahan et al. (1996) function is needed, in order to bring it to Mårtensson et al. (2003) range.

5 SSA and climate change: production, fate and radiative impact

The regional-scale impact of SSA production and fate caused by a changing climate has been shown in Sect. 3. We show that the change in SSA emission between the past and future periods is not so large, arguably due to the small change in wind speed between the two time periods. Climates studies such as Gregow et al. (2011) projected higher wind speed changes in periods closer to the years 2100, in Scandinavia. Nevertheless, the available climate estimations of wind can differ substantially given the little understanding of how wind speed may change over the ocean in a warmer climate (IPCC, 2013). Studies such as Salisbury et al. (2013) suggest that other variables, in addition to wind forcing, influence the whitecap fraction, such as the seawater temperature or the sea state. New parameterization for whitecap fraction, based on satellite observations, claims that the whitecap-area based parameterization used by all the models in this study is misrepresenting the absolute values. Albert et al. (2015) suggests that for higher latitudes the values are overestimated, and underestimated for lower latitudes. If following that parameterization, the emission over the Mediterranean is underestimated. This could mean that the changes in seawater temperature would impact the SSA emission flux more substantially than suggested by this study.

The aerosol direct radiative effect (DRE) is defined as the difference between net radiative fluxes at TOA in the presence and absence of SSA. The radiative forcing depends on the AOD of the aerosol species in the atmosphere, the surface albedo and the vertical position of clouds. In this study, all-sky conditions were considered, i.e. clouds are included. Over the seawater surfaces, SSA directly scatters solar radiation back to space, resulting in a cooling effect on the climate by decreasing the amount of radiation absorbed by the water surface. Over land, there can be both cooling over the low-reflectance surfaces, and warming over high-albedo surfaces (e.g., Haywood and Boucher, 2000). Adding only a low absorbing aerosol, such as SSA, and assuming the same atmospheric and

Atmos. Chem. Phys. Discuss., doi:10.5194/acp-2015-1056, 2016
Manuscript under review for journal Atmos. Chem. Phys.
Published: 16 February 2016

555 cloud conditions for the all the runs (with and without SSA), the upward scattering by SSA will be
556 the only radiation impact in this study.

557 Figure 12 shows the DRE due to SSA in the past (left panel) and the change in DRE due to the
558 changing climate (right panel). These calculations are based on the AOD predicted by SILAM for
559 the past and future. As expected, the past computations predict the highest cooling effect due to
560 SSA over the areas where concentrations (Fig. 7, left-lower panel) are the highest and where the
561 surface albedo is the lowest (seawater surfaces). The strongest effect is seen over the Mediterranean
562 Sea due to the lowest cloud cover and the largest number of hours of sunlight per year. Studies such
563 as Ma et al. (2008) and Lundgren et al. (2013), state that the impact of clouds can be substantial,
564 reducing the direct radiative impact of SSA. The lowest cooling effect is predicted over land where
565 the albedo is higher and SSA amount is the lowest. Conversely, warming is predicted where the
566 albedo is high and the AOD is low, e.g. over the mountain tops in Norway and Italy. The current
567 study estimates the upward scattering by SSA, at TOA, to be up to 0.5 W m^{-2} over seawater
568 surfaces. This value is within the estimates on upward scattering of radiation by SSA: ranging
569 between 0.08 and 6 W m^{-2}, at wavelengths in the range of 0.3-4 µm (Lewis and Schwartz, 2004).

570 Figure2, right panel, depicts the change in the DRE due to SSA between future and past. The results
571 suggest overall cooling (negative change) in the future: North of Iceland, Norwegian and North
572 Seas are the areas where the cooling is more accentuated. The Mediterranean area seems to be again
573 the most sensitive area in our study: it is predicted an overall warming for this area, both over sea
574 and over land, but also cooling, in particular in the east of the eastern basin. DRE pattern for the
575 whole year is highly influenced by the summer period due to largest number of daylight hours. This
576 can be seen in Fig. 13, right panel, which shows the change between future and past but considering
577 only the summer months (JJA). This study predicts a substantial seasonal variation for the DRE in
578 the sea surface waters. This is expected due to the variation shown in Sect. 3.2 and 3.3. The upward
579 scattering in the summer time can be up to 1.7 times higher than in winter, due to lower cloudiness
580 and lengthier daylight.

581 Figure 13 shows the change in winter (left panel) and summer (right) between the future and the
582 past. The strongest impact in winter is seen over the Mediterranean area: negative over the sea
583 surface and positive over land. In summer, the highest impact is over the seawater surfaces,
584 predicting a cooling effect in the future, with exception over the western basin of the Mediterranean
585 and the western side of the British Isles and France.

Atmos. Chem. Phys. Discuss., doi:10.5194/acp-2015-1056, 2016
Manuscript under review for journal Atmos. Chem. Phys.
Published: 16 February 2016

The results presented in this study for the present period are in accordance with the regional simulations for a summer month presented by Lundgren et al (2013) and the global simulations presented by, e.g. Grini et al. (2002) and Ma et al. (2008). The results are shown in Table 5.

The radiative forcing calculation is also sensitive to the SSA single scattering albedo. Thus, setting the SSA's single scattering albedo as low as 0.95 (Russel et al, 2002), leads to a wide areas over land where warming is substantial: essentially, over all surfaces with albedos exceeding 0.5 and low (<0.03) aerosol load (not shown). We have chosen to show results for a more realistic SSA single scattering albedo of 0.99 (Lundgren et al., 2013).

6 Conclusion

This study has compared predictions of SSA emissions, surface concentration and deposition from four CTMs for both current condition and future scenarios, focusing on the European Seas: Baltic, North, Mediterranean, and Black Seas. The three European-scale CTMs (EMEP, MATCH and SILAM) were driven by the regional climate model (RCA3) meteorology and by the hemispheric model (DEHM) boundary conditions. The hemispheric model was driven by the ECHMA5 meteorology. The impact of climate change on SSA production and fate, due to changes in wind speed and seawater temperature, was analysed. Additionally, consideration about the impact of seawater salinity on emissions was given.

The impact of climate change on SSA production and fate has different response from the models, with the similar results between DEHM and EMEP, and between MATCH and SILAM. DEHM-EMEP show almost no difference between future and past periods, and MATCH-SILAM shows a general increase of the emissions and surface concentrations with levels reaching 30% in change. The emissions increase is substantial in the Black Sea, Gulf of Bothnia (Baltic) and Levantine Sea (Mediterranean), correlating well with the wind-forcing ($\approx U_{10}^{3.41}$) computed with the changes predicted between the same periods. Nevertheless, the major driver of the changes of the sea-salt fluxes from the sea surface will be the changing seawater temperature, since near-surface wind speed is projected to stay nearly the same in the climate scenario used, in absolute levels the wind will change less than a meter per second, in average, between the two periods. The concentrations are predominantly increasing in Black and Mediterranean Sea. The impact of climate change on SSA on deposition is not really relevant; though an increase is projected around Iceland by all the models. Boundary conditions impact on the predictions is substantial.

The discrepancies between the models raised additional question about the implementation of the SSA production formulations, since three of the models are based on the same parameterizations. This study shows that the way a given parameterizations is implemented in the models and the temperature and salinity correction functions play an important role for the final scaling of the SSA flux: size range prescription may play a substantial role on the SSA flux calculation.

Simple calculations with the libRadTran allowed understanding the impact of SSA on the direct radiative forcing. According to this study the upward scattering by SSA, at TOA, can to be up to 0.5 W m^{-2} over the seawater surfaces in the present period, predicting an overall cooling in the future. The most affected areas by cooling will be North of Iceland, Norwegian and North Seas, and the eastern basin of the Mediterranean; warming is predicted manly in Mediterranean Sea, including over land.

Acknowledgements

This study was supported by the Nordic Council of Ministers, EnsCLIM and CarboNord projects. The authors also thank Antti Arola for his guidance in the radiative forcing calculations and interpretation of the results.

References

Albert, M. F. M. A., Anguelova, M. D., Manders, A. M. M., Schaap, M., and de Leeuw, G.: Parameterization of oceanic whitecap fraction based on satellite observations, Atmos. Chem. Phys. Discuss., 15, 21219-21269, doi:10.5194/acpd-15-21219-2015, 2015.

Andersson, C., Bergström, R., Bennet, C., Robertson, L., Thomas, M., Korhonen, H., Lehtinen, K. E. J., and Kokkola, H.: MATCH-SALSA – Multi-scale Atmospheric Transport and CHemistry model coupled to the SALSA aerosol microphysics model – Part 1: Model description and evaluation, Geosci. Model Dev., 8, 171-189, doi:10.5194/gmd-8-171-2015, 2015.

Andreas, E. L.: A new sea spray generation function for wind speeds up to 32 m s−1, J. Phys. Oceanogr., 28, 2175–2184, doi:10.1175/1520-0485(1998)028<2175:ANSSGF>2.0.CO;2., 1998

Andreas, E. L., Edson, J. B., Monahan, E. C., Rouault, M. P., and Smith, S. D.: The spray contribution to net evaporation from the sea: A review of recent progress, Boundary Layer Meteorol., 72(1–2), 3–52, doi:10.1007/BF00712389, 1995.

647 Bates, T. S., Coffman, D. J., Covert, D. S., and Quinn, P. K.: Regional marine boundary layer
648 aerosol size distributions in the Indian, Atlantic, and Pacific Oceans: A comparison of INDOEX
649 measurements with ACE-1, ACE-2, and Aerosols99, J. Geophys. Res., 107(D18), 8026,
650 doi:10.1029/2001JD001174, 2002.

651 Bellouin, N., Rae, J., Jones, A., Johnson, C., Haywood, J., and Boucher, O.: Aerosol forcing in the
652 Climate Model Intercomparison Project (CMIP5) simulations by HadGEM2-ES and the role of
653 ammonium nitrate, J. Geophys. Res., 116, D20206, doi:10.1029/2011JD016074, 2011.

654 Boyer, T. P., Levitus S., Garcia, H. E., Locarnini, R. A., Stephens, C., Antonov, J. I.; Objective
655 analyses of annual, seasonal, and monthly temperature and salinity for the world ocean on a 0.25
656 degrees grid. Int. J. Climatol. 25 (7), 931-945, 2005.

657 Boyd, P. W.: Ranking geo-engineering schemes, Nat. Geosci., 1, 722–724, doi:10.1038/ngeo348,
658 2008.

659 Brandt J, Brandt, J., Silver, J., Frohn, L. M., Geels, C., Gross, A., Hansen, A. B., Hansen, K. M.,
660 Hedegaard, G. B., Skjøth, C. A., Villadsen, H., Zare, A., and Christensen, J. H.: An integrated
661 model study for Europe and North America using the Danish Eulerian Hemispheric Model with
662 focus on intercontinental transport of air pollution. Atmos.Environ. 53:156-176, 2012.

663 Covert, D. S., Gras, J. L, Wiedensohler, A., and Stratmann, F.: Comparison of directly measured
664 CCN with CCN modeled from the number-size distribution in the marine boundary layer during
665 ACE I at Cape Grim, Tasmania, J. Geophys. Res., 103, 16,597-16,608, 1998.

666 de Leeuw, G., Andreas, E. L, Anguelova, M. D., Fairall, C. W., Lewis, E. R., O'Dowd, C., Schulz,
667 M. and Schwartz, S. E.: Production flux of sea spray aerosol, Rev. Geophys., 49, RG2001,
668 doi:10.1029/2010RG000349, 2011.

669 Dana, M. T., and Hales, J. M.; Statistical aspects of the washout of polydisperse aerosols. Atmos.
670 Environ. 10, 45-50, 1976.

671 Emberson, L. D., Ashmore, M. R., Cambridge, H. M., Simpson, D., and Tuovinen, J. P.: Modelling
672 stomatal ozone flux across Europe, Environ. Pollut., 109, 403–413, 2000.

673 Foltescu, V. L., Pryor, S. C. and Bennet, C.: Sea salt generation, dispersionand removal on the
674 regional scale. Atmospheric Environment 39, 2123-2133, 2005.

675 Gregow, H., Ruosteenoja, K., Pimenoff, N., and Jylhä, K.: Changes in the mean and extreme
676 geostrophic wind speeds in Northern Europe until 2100 based on nine global climate models. Int.
677 J. Climatol., 32, 1834–1846, 2011.

678 Grini, A., Myhre, G., Sundet, J. K., and Isaksen, I. S. A.: Modeling the annual cycle of sea salt in
679 the global 3D model OsloCTM2: Concentrations, fluxes, and radiative impact, J. Climate, 15,
680 1717–1730, 2002.

681 Gong, S. L.: A parameterization of sea-salt aerosol source function for sub- and super-micron
682 particles, Global Biogeochem. Cycles, 17(4), 1097, doi:10.1029/2003GB002079, 2003.

683 Gong, S. L., Barrie, L. A., Prospero, J. M., Savoie, D. L., Ayers, G. P., Blanchet, J.-P., and Spacek,
684 L.: Modelling sea-salt aerosols in the atmosphere: 2. Atmospheric concentrations and fluxes, J.
685 Geophys. Res., 102(D3), 3819–3830, doi:10.1029/96JD03401, 1997.

686 Haywood, J., and Boucher, O.: Estimates of the direct and indirect radiative forcing due to
687 tropospheric aerosols: A review, Rev. Geophys., 38(4), 513–543, doi:10.1029/1999RG000078,
688 2000.

689 Haywood, J., Ramaswamy, V., and Soden, B.: Tropospheric aerosol climate forcing in clear-sky
690 satellite observations over the oceans, Science, 283, 1299– 1303, 1999.

691 Hjellbrekke, A.-G. & Fjæra, A. M.: Data Report: Acidifying and eutrophying compounds and
692 particulate matter. EMEP/CCC-Report 1/2011, 2009.

693 Horn, H., Bonka, H., and Maqua, M.: Measured particle bound activity size-distribution, deposition
694 velocity, 700 and activity concentration in rainwater after the Chernobyl accident, J. of Aerosol
695 Science, 18, 681–684, 10.1016/0021-8502(87)90096-6, 1987.

696 Huebert, B. J., Bates, T., Russell, P. B., Shi, G., Kim, Y. J., Kawamura, K., Carmichael, G., and
697 Nakajima, T.: An overview of ACE-Asia: Strategies for quantifying the relationships between
698 Asian aerosols and their climatic impacts, J. Geophys. Res., 108(D23), 8633,
699 doi:10.1029/2003JD003550, 2003.

700 IPCC: Climate Change 2013: The Physical Science Basis. Contribution of Working Group I to the
701 Fifth Assessment Report of the Intergovernmental Panel on Climate Change [Stocker, T.F., D.
702 Qin, G.-K. Plattner, M. Tignor, S.K. Allen, J. Boschung, A. Nauels, Y. Xia, V. Bex and P.M.
703 Midgley (eds.)]. Cambridge University Press, Cambridge, United Kingdom and New York, NY,
704 USA, 1535 pp, doi:10.1017/CBO9781107415324, 2013

705 Jylhä, K.: Empirical scavenging coefficients of radioactive substances released from Chernobyl,
706 Atmos. Environ. A., 25, 263–270, 10.1016/0960-1686(91)90297-K, 1991.

707 Kjellström, E., Nikulin, G., Hansson, U., Strandberg, G., and Ullerstig, A.: 21st century changes in
708 the European climate: uncertainties derived from an ensemble of regional climate model
709 simulations, Tellus Series A-Dynamic Meteorology and Oceanography, 63, 24–40,
710 10.1111/j.1600-0870.2010.00475.x, 2011.

711 Kaskaoutis, D. G., Kambezidis, H. D., Hatzianastassiou, N., Kosmopoulos, P. G., and
712 Badarinath, K. V. S.: Aerosol climatology: dependence of the Angstrom exponent on wavelength
713 over four AERONET sites, Atmos. Chem. Phys. Discuss., 7, 7347-7397, doi:10.5194/acpd-7-
714 7347-2007, 2007.

715 Kusmierczyk-Michulec J. and van Eijk, A.M.J.: Atmospheric Optics: Models, Measurements, and
716 Target-in-the-Loop Propagation III, 74630G; Stephen M. Hammel; Alexander M. J. van Eijk;
717 Mikhail A. Vorontsov, Editor(s) doi: 10.1117/12.828394, 2009.

718 Korhonen, H., K. Carslaw, S., and Romakkaniemi, S.: Enhancement of marine cloud albedo via
719 controlled sea spray injections: A global model study of the influence of emission rates,
720 microphysics and transport, Atmos. Chem. Phys., 10, 4133–4143, doi:10.5194/acp-10-4133-
721 2010, 2010.

722 Kouznetsov, R. and Sofiev, M.: A methodology for evaluation of vertical dispersion and dry
723 deposition of atmospheric aerosols, J. Geophys. Res., 117, 10.1029/2011JD016366, 2012.

724 Langner, J., Engardt, M., and Andersson, C.: European summer surface ozone 1990–2100, Atmos.
725 Chem. Phys., 12, 10097-10105, doi:10.5194/acp-12-10097-2012, 2012.

726 Latham, J., and Smith, M. H.: Effect on global warming of wind dependent aerosol generation at the
727 ocean surface, Nature, 347, 372–373, doi:10.1038/347372a0, 1990.

728 Lenton, T. M., and Vaughan, N. E.: The radiative forcing potential of different climate
729 geoengineering options, Atmos. Chem. Phys., 9, 5539–5561, doi:10.5194/acp-9-5539-2009,
730 2009.

731 Lewis, E. R., and Schwartz, S. E.: Comment on "Size distribution of sea-salt emissions as a
732 function of relative humidity," Atmos. Environ., 40, 588–590,
733 doi:10.1016/j.atmosenv.2005.08.043, 2006.

734 Liao, H., Chen, W. T., and Seinfeld, J. H.: Role of climate change in global predictions of future
735 tropospheric ozone and aerosols. J. Geophys. Res., 111, D12304, 2006.

736 Lundgren, K., Vogel, B.,Vogel, H., and Kottmeier, C.: Direct radiative effects of sea salt for the
737 Mediterranean region under conditions of low to moderate wind speeds, J. Geophys. Res.
738 Atmos., 118, 1906–1923, doi:10.1029/2012JD018629, 2013.

739 Ma, X., von Salzen, K., and Li, J.: Modelling sea salt aerosol and its direct and indirect effects on
740 climate, Atmos. Chem. Phys., 8, 1311-1327, doi:10.5194/acp-8-1311-2008, 2008.

741 Mahowald, N. M., Lamarque, J.-F., Tie, X. X., and Wolff, E.: Sea-salt aerosol response to climate
742 change: Last Glacial Maximum, preindustrial, and doubled carbon dioxide climates, J. Geophys.
743 Res., 111, D05303, doi:10.1029/2005JD006459, 2006.

744 Manders, A. M. M., Schap, M., Querol, X., Albert, M. F., Vercauteren, J., Kuhlbusch, T. A. J., and
745 Hoogerbrugge, R.: Sea salt concentrations across the European continent, Atmos. Environ., 44,
746 2434–2442, doi:10.1016/j.atmosenv.2010.03.028, 2010.

747 Mayer, B. and Kylling, A.: Technical note: The libRadtran software package for radiative transfer
748 calculations - description and examples of use, Atmos. Chem. Phys., 5, 1855-1877,
749 doi:10.5194/acp-5-1855-2005, 2005.

750 Mie, G.: Beiträge zur Optik trüber Medien, speziell kolloidaler Metallösungen [Contribution to the
751 optics of turbid media, particularly of colloquial metal solutions Royal Aircraft Establishment],
752 Ann. Phys.25(3), 377–445, 1908.

753 Monahan, E. C., Spiel, D. E., and Davidson, K. L.: A model of marine aerosol generation via
754 whitecaps and wave disruption, in Oceanic Whitecaps, edited by E. C. Monahan and G.
755 MacNiochaill, 167–193, D. Reidel, Norwell, Mass, 1986.

756 Mårtensson, E. M., Nilsson, E. D., de Leeuw, G., Cohen, L. H., and Hansson, H.-C.: Laboratory
757 simulations and parameterization of the primary marine aerosol production, J. Geophys. Res.,
758 108(D9), 4297, doi:10.1029/2002JD002263, 2003

759 Nakićenović, N.: Global greenhouse gas emissions scenarios: Integrated modeling approaches,
760 Tech. Forecasting & Social Change, 63, 105–109, 2000.

761 Nilsson, E. D., Mårtensson, E. M., van Ekeren, J. S., de Leeuw, G., Moerman, M. M., and O'Dowd,
762 C. D.: Primary marine aerosol emissions: Size resolved eddy covariance measurements with

763 estimates of the sea salt and organic carbon fractions, Atmos. Chem. Phys. Discuss., 7, 13,345–
764 13,400, doi:10.5194/acpd-7-13345-2007, 2007.

765 NOAA: World Ocean Atlas 2013. http://www.nodc.noaa.gov/OC5/woa13/, 2013

766 O'Dowd, C., and de Leeuw, G.: Marine aerosol production: A review of the current knowledge,
767 Philos. Trans. R. Soc. A, 365, 1753–1774, doi:10.1098/rsta.2007.2043, 2007.

768 O'Dowd, C. D., and Smith, M. H.: Physico-chemical properties of aerosol over the North East
769 Atlantic: Evidence for wind speed related sub-micron sea-salt aerosol production, J. Geophys.
770 Res., 98, 1137–l149, doi:10.1029/92JD02302, 1993.

771 O'Dowd, C., Lowe, J., Smith, M., and Kaye, A.: The relative importance of non-seasalt sulphate
772 and sea-salt aerosol to the marine cloud condensation nuclei population: An improved multi-
773 component aerosolcloud droplet parameterization, Q. J. R. Meteorol. Soc., 125, 1295–1313,
774 1999.

775 O'Dowd, C. D., Smith, M. H. Consterdine, I. E., and Lowe, J. A.: Marine aerosol, sea salt, and the
776 marine sulphur cycle: A short review, Atmos. Environ., 31, 73–80, doi:10.1016/S1352-
777 2310(96)00106-9, 1997

778 Ovadnevaite, J., Manders, A., de Leeuw, G., Ceburnis, D., Monahan, C., Partanen, A.-I., Korhonen,
779 H., and O'Dowd, C. D.: A sea spray aerosol flux parameterization encapsulating wave state,
780 Atmos. Chem. Phys., 14, 1837-1852, doi:10.5194/acp-14-1837-2014, 2014.

781 Pierce, J. R., and Adams, P. J.: Global evaluation of CCN formation by direct emission of sea salt
782 and growth of ultrafine sea salt, J. Geophys. Res., 111, D06203, doi:10.1029/2005JD006186,
783 2006.

784 Pincus, R., Platnick, S., Ackerman, S. A., Hemler, R. S., and Hofmann, R. J. P.: Reconciling
785 simulated and observed views of clouds: MODIS, ISCCP, and the limits of instrument
786 simulators, Journal of Climate, 2011.

787 Pryor, S. C., and Barthelmie, R. J.: Particle dry deposition to water surfaces: processes and
788 consequences. Marine Pollution Bulletin 41, 220-231, 2000.

789 Prank, M.: Evaluation of atmospheric composition simulations via comparison with remote-sensing
790 and in-situ observations, Master's thesis, 74 pp., Dep. of Sci. and Technol., Univ. of Tartu,
791 Tartu, Estonia, 2008.

792 Quinn, P. K., Coffman, D. J., Kapustin, V. N., Bates, T. S., Covert, D. S.: Aerosol optical properties
793 in the marine boundary layer during the First Aerosol Characterization Experiment (ACE 1) and
794 the underlying chemical and physical aerosol properties, J. Geophys. Res., 103, D13, 547-
795 16,563, 1998

796 Roeckner, E., Brokopf, R., Esch, M., Giorgetta, M., Hagemann, S., Kornblueh, L., Manzini, E.,
797 Schlese, U., and Schulzweida, U.: Sensitivity of simulated climate to horizontal and vertical
798 resolution in the ECHAM5 atmosphere model, J. Clim., 19, 3771–3791, 10.1175/JCLI3824.1,
799 2006.

800 Rodell, M., Houser, P.R., Jambor, U., Gottschalck, J., Mitchell, K., Meng, C.-J., Arsenault, K.
801 Cosgrove, B., Radakovich, J., Bosilovich, M., Entin, J.K., Walker, J.P., Lohmann, D., and Toll,
802 D.: The Global Land Data Assimilation System, Bull. Amer. Meteor. Soc., 85(3), 381-394, 2004

803 Russel, P.B., and Heintzenberg, J.: An overview of the ACE-2 clear sky column closure experiment
804 (CLEARCOLUMN). Tellus B, [S.l.], 52(2), ISSN 1600-0889,
805 doi:http://dx.doi.org/10.3402/tellusb.v52i2.16173, 2011.

806 Russell, P. B., Redemann, J., Schmid, B., Bergstrom., R. W., Livingston, J. M., McIntosh, D. M.,
807 Ramirez, S. A., Hartley, S., Hobbs, P. V., Quinn, P. K., Carrico, C. M., Rood, M. J., Öström, E.,
808 Noone, K. J., von Hoyningen-Huene, W., and Remer, L.: Comparison of Aerosol Single
809 Scattering Albedos Derived by Diverse Techniques in Two North Atlantic Experiments. J.
810 Atmos. Sci., 59, 609–619, doi: http://dx.doi.org/10.1175/1520-
811 0469(2002)059<0609:COASSA>2.0.CO;2, 2002

812 Salisbury, D. J., Anguelova, M. D., and Brooks, I. M.: On the variability of whitecap fraction using
813 satellite-based observations, J. Geophys. Res.-Oceans, 118, 6201–6222, 2013.

814 Samuelsson, Jones, P., Willén, C. G., Ullerstig, U., Gollvik, A., Hansson, S., Jansson, U.,
815 Kjellström, C., Nikulin, E., and Wyser, K.: The Rossby Centre Regional Climate model RCA3:
816 Model description and performance, Tellus A, 63, 4–23, doi:10.111/j.1600-0870.2010.00478.x,
817 2011.

818 Seinfield, J. H., and Pandis, S. N.: Atmospheric Chemistry and Physics: From Air Pollution to
819 Climate Change, 2nd ed., 1232, John Wiley, Hoboken, N. J., 2006.

820 Simpson, D., Andersson, C., Christensen, J.H., Engardt, M., Geels, C., Nyiri, A., Posch, M., Soares,
821 J., Sofiev, M., Wind, P., and Langner, J.: Impacts of climate and emission changes on nitrogen

deposition in Europe: a multi-model study, Atmos. Chem. Phys., 14, 6995-7017, doi:10.5194/acp-14-6995-2014, 2014.

Simpson, D., Fagerli, H., Jonson, J. E., Tsyro, S., Wind, P., and Tuovinen, J.-P: Transboundary Acidification, Eutrophication and Ground Level Ozone in Europe, PART I, Unified EMEP Model Description, 1-104, 2003.

Smith, F. B., and Clark, M. J.: The transport and deposition of radioactive debris from the Chernobyl nuclear power plant accident with special emphasis on consequences to the United Kingdom, Meteorological Office Scientific Paper no. 42, HMSO London, 1989.

Sofiev, M., Siljamo, P., Valkama, I., Ilvonen, M., and Kukkonen, J.: A dispersion modelling system SILAM and its evaluation against ETEX data, Atmos. Environ., 40, 674–685, 10.1016/j.atmosenv.2005.09.069, 2006.

Sofiev, M., Soares, J., Prank, M., de Leeuw, G., and Kukkonen, J.: A regional-to-global model of emission and transport of sea salt particles in the atmosphere, J. Geophys. Res., 116, D21302, doi:10.1029/2010JD014713, 2011.

Struthers, H., Ekman, A. M. L., Glantz, P., Iversen, T., Kirkevåg, A., Mårtensson, E. M., Seland, Ø., and Nilsson, E. D.: The effect of sea ice loss on sea salt aerosol concentrations and the radiative balance in the Arctic, Atmos. Chem. Phys., 11, 3459-3477, doi:10.5194/acp-11-3459-2011, 2011.

Tsyro, S., Aas, W., Soares, J., Sofiev, M., Berge, H., and Spindler, G.: Modelling of sea salt pollution over Europe: key uncertainties and comparison with observations Atmos. Chem. Phys., 11, 10367-10388, doi:10.5194/acp-11-10367-2011, 2011.

Textor, C., Schulz, M., Guibert, S., Kinne, S., Balkanski, Y., Bauer, S., Berntsen, T., Berglen, T., Boucher, O., Chin, M., Dentener, F., Diehl, T., Easter, R., Feichter, H., Fillmore, D., Ghan, S., Ginoux, P., Gong, S., Grini, A., Hendricks, J., Horowitz, L., Huang, P., Isaksen, I., Iversen, I., Kloster, S., Koch, D., Kirkevåg, A., Kristjansson, J. E., Krol, M., Lauer, A., Lamarque, J. F., Liu, X., Montanaro, V., Myhre, G., Penner, J., Pitari, G., Reddy, S., Seland, Ø., Stier, P., Takemura, T., and Tie, X.: Analysis and quantification of the diversities of aerosol life cycles within AeroCom, Atmos. Chem. Phys., 6, 1777-1813, doi:10.5194/acp-6-1777-2006, 2006.

Twomey S.: Atmospheric Aerosol, Elviser, Amesterdam, 1977.

851 Tørseth, K., Aas, W., Breivik, K., Fjæraa, A. M., Fiebig, M., Hjellbrekke, A. G., Lund Myhre, C.,
852 Solberg, S., and Yttri, K. E.: Introduction to the European Monitoring and Evaluation
853 Programme (EMEP) and observed atmospheric composition change during 1972–2009, Atmos.
854 Chem. Physics, 12, 5447–5481, 10.5194/acp-12-5447-2012, http://www.atmos-chem-
855 phys.net/12/5447/2012/, 2012.

856 Wang, M., Ghan, S., Ovchinnikov, M., Liu, X., Easter, R., Kassianov, E., Qian, Y., and Morrison,
857 H.: Aerosol indirect effects in a multi-scale aerosol-climate model PNNL-MMF, Atmos. Chem.
858 Phys., 11, 5431-5455, doi:10.5194/acp-11-5431-2011, 2011.

859 Witek, M. L., P. J. Flatau, J. Teixeira, and K. M. Markowicz: Numerical investigation of sea salt
860 aerosol size bin partitioning in global transport models: Implications for mass budget and optical
861 depth, Aerosol Sci. Technol., 45, 401–414, doi:10.1080/02786826.2010.541957, 2011.

862 Witek, M. L., Flatau, P. J., Quinn, P. K., and Westphal, D. L.: Global sea-salt modeling: Results
863 and validation against multicampaign shipboard measurements, J. Geophys. Res., 112, D08215,
864 doi:10.1029/2006JD007779, 2007a.

865 Witek, M. L., Flatau, P. J., Teixeira, K., and Westphal, D. L: Coupling an ocean wave model with a
866 global aerosol transport model: A sea salt aerosol parameterization perspective, Geophys. Res.
867 Lett., 34, L14806, doi:10.1029/2007GL030106, 2007b.

868 van Loon, M., Tarrasón, L., and Posch, M.: Modelling Base Cations in Europe, Technical Report
869 MSC-W, Norwegian Meteorological Institute, ISSN 0804-2446, 2005

870 Zhang, L., Gong, S., Padro, J., and Barrie, L.: A size-segregated particle dry deposition scheme for
871 an atmospheric aerosol module. Atmospheric Environment 35, 549-560., 2001.

872

873

Atmos. Chem. Phys. Discuss., doi:10.5194/acp-2015-1056, 2016
Manuscript under review for journal Atmos. Chem. Phys.
Published: 16 February 2016

Atmospheric Chemistry and Physics Discussions

874 Table 1 Model characteristics for SSA computations.

model	mode	Dp [µm]	source function	dependency	humidity	Lowest model layer thickness (m)
DEHM	fine	<1.3	MA02	T S	static (80%)	60
	coarse	[1.3-10]	MO86	S		
EMEP	fine	<2.5	MA02	T	static (80%)	90
	coarse	[2.5-10]	MO86	-		
MATCH	fine	[0.02–0.1]	MA02	T S	dynamic	60
		[0.1–1]				
		[1–2.5]				
	coarse	[2.5–10]	MO86	T (SO11) S		
SILAM	fine	[0.01–0.1]	SO11	T S	dynamic	25
		[0.1–1.5]				
	coarse	[1.5–6]				
		[6–15]	SO11	T S		
		[15-30]				

875 **T**: temperature, **S**: salinity, **MO86**: Monahan et al. (1986); **MA03**: Mårtensson et al. (2003), **SO11**:
876 Sofiev et al. (2011). In bold, the modes not used for the PM_{10} analysis.
877
878
879

Atmos. Chem. Phys. Discuss., doi:10.5194/acp-2015-1056, 2016
Manuscript under review for journal Atmos. Chem. Phys.
Published: 16 February 2016

Atmospheric Chemistry and Physics Discussions

880 Table 2 Assumption for the radiative transfer modelling libRadTran2.0 for present and future.

Clouds (icy and wet)	cloud cover	monthly averaged RCA3 fields (1990-2009); same for both periods
	AOD	monthly averaged MODIS data (2002-2014) (Pincus et al. 2011); same for both periods
	vertical profiles	wc.dat*; wc.dat*
Atmospheric properties	vertical profiles	subarctic winter, latitude over 60°: afglsw.dat* subarctic summer, latitude over 60°: afglss.dat* mid-latitude winter, latitude below 60°: afglmw.dat* mid-latitude summer, latitude below 60°: afglms.dat*
	altitude, pressure and temperature	monthly averaged RCA3 fields (1990-2009); same for both periods
Aerosol properties	vertical profile	aerosol_default*
	AOD	dynamic: SILAM AOD calculations
	asymmetry factor	0.8 (Ma et al. 2008)
	single scattering albedo	0.99 (Lundgren et al, 2013)
	angstrom coefficient	0.2 (Kaskaoutis et al, 2007; Kusmierczyk-Michulec & van Eijk, 2009)
solar zenith angle		dynamic: computed with libRadTran sza tool
surface albedo		monthly averaged NOAA data (1990-2012) (Rodell et al., 2004); same for both periods
RTE solver		DISORT
integrated shortwave calculation scheme		KATO2 (wavelength ~[0.2, 4] μm)

881 *standard file in libRadTran

882

Atmos. Chem. Phys. Discuss., doi:10.5194/acp-2015-1056, 2016
Manuscript under review for journal Atmos. Chem. Phys.
Published: 16 February 2016

Atmospheric Chemistry and Physics Discussions

883 Table 3 Statistical evaluation of model results for surface SSA concentration (Na^+µg m^{-3}),
884 considering the whole year (annual), winter (December, January and February) and summer
885 periods (June, July and August), for 33 EMEP measuring sites, between 1990 and 2009.

	annual	**winter**	**summer**	**annual**	**winter**	**summer**
Obs	0.72	0.94	0.55			
DEHM	1.08	1.39	0.74			
EMEP	0.64	0.75	0.49			
MATCH	0.45	0.42	0.42			
SILAM	0.86	0.78	0.94			
		correlation			StdRatio	
DEHM	0.85	0.87	0.81	1.72	1.57	1.79
EMEP	0.82	0.84	0.80	0.69	0.54	0.85
MATCH	0.75	0.82	0.77	0.48	0.33	0.66
SILAM	0.71	0.77	0.75	1.05	0.75	1.59
		RMSE			Bias	
DEHM	0.97	1.11	0.70	0.36	0.45	0.18
EMEP	0.53	0.75	0.36	-0.08	-0.18	-0.06
MATCH	0.69	1.03	0.41	-0.27	-0.52	-0.14
SILAM	0.71	0.76	0.74	0.14	-0.16	0.38

886
887

Atmos. Chem. Phys. Discuss., doi:10.5194/acp-2015-1056, 2016
Manuscript under review for journal Atmos. Chem. Phys.
Published: 16 February 2016

Atmospheric Chemistry and Physics Discussions

888 Table 4 Statistical evaluation of model results for SSA wet deposition (Na^+mg m^{-2}), considering
889 the whole year (annual), winter (December, January and February) and summer periods (June, July
890 and August) for 133 EMEP measurement sites, between 1990 and 2009. SILAM5m is the
891 evaluation if considering the whole possible size range for SSA Dp = [0.01-30] µm.

	annual	**winter**	**summer**	**annual**	**winter**	**summer**
obs	1.59E+06	6.88E+05	1.36E+05			
DEHM	1.41E+06	5.59E+05	1.40E+05			
EMEP	1.64E+06	6.44E+05	1.65E+05			
MATCH	6.08E+05	1.77E+05	9.64E+04			
SILAM	8.42E+05	2.81E+05	1.25E+05			
SILAM5m	1.70E+06	6.70E+05	1.83E+05			
		correlation			StdRatio	
DEHM	0.55	0.53	0.41	0.36	0.31	0.55
EMEP	0.38	0.32	0.33	0.47	0.44	0.53
MATCH	0.49	0.50	0.34	0.13	0.11	0.26
SILAM	0.49	0.45	0.38	0.22	0.19	0.41
SILAM5m	0.62	0.63	0.37	0.86	0.84	0.93
		RMSE			Bias	
DEHM	3477	5513	866	-114	-327	10
EMEP	3778	6006	912	34	-112	74
MATCH	3879	6122	892	-634	-1304	-102
SILAM	3737	5945	871	-483	-1038	-29
SILAM5m	3335	5070	1032	73	-44	122

892
893

Atmos. Chem. Phys. Discuss., doi:10.5194/acp-2015-1056, 2016
Manuscript under review for journal Atmos. Chem. Phys.
Published: 16 February 2016

Atmospheric Chemistry and Physics Discussions

894 Table 5 Predicted direct radiative effect (W m^{-2}) by SSA for the past period

	annual	**winter**	**summer**
sea	-0.25±0.22	-0.077±0.053	-0.21±0.012
land	-0.20±0.18	-0.073±0.0019	-0.083±0.0030

895

Atmos. Chem. Phys. Discuss., doi:10.5194/acp-2015-1056, 2016
Manuscript under review for journal Atmos. Chem. Phys.
Published: 16 February 2016

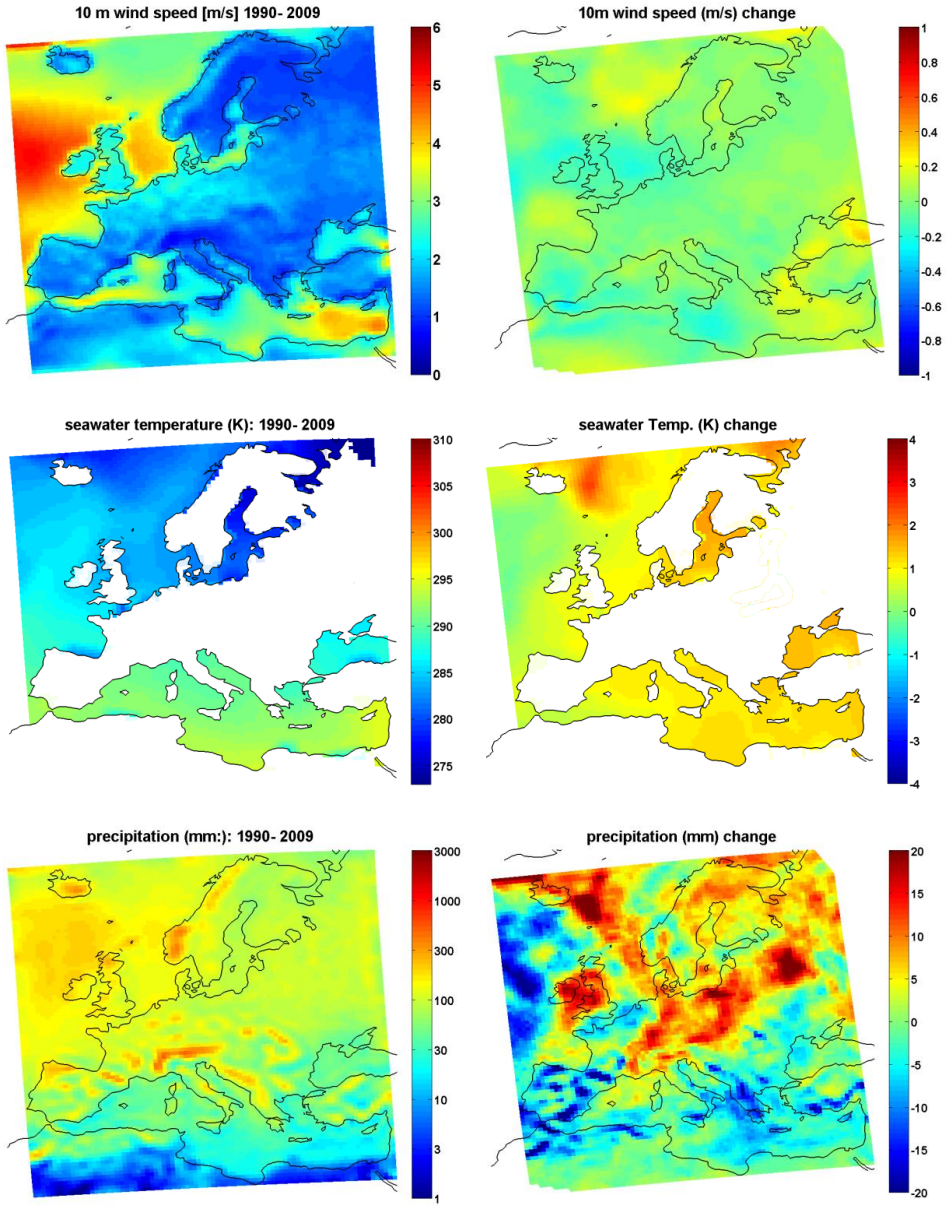

896

897 Figure 1. Top: Sea surface temperature (K), middle: wind speed (m s^{-1}), bottom: precipitation (mm). Left
898 panel: mean value for the past period (1990-2009); right panel: absolute difference between the future (2040-
899 2059) and past periods.

Atmos. Chem. Phys. Discuss., doi:10.5194/acp-2015-1056, 2016
Manuscript under review for journal Atmos. Chem. Phys.
Published: 16 February 2016

Atmospheric Chemistry and Physics Discussions

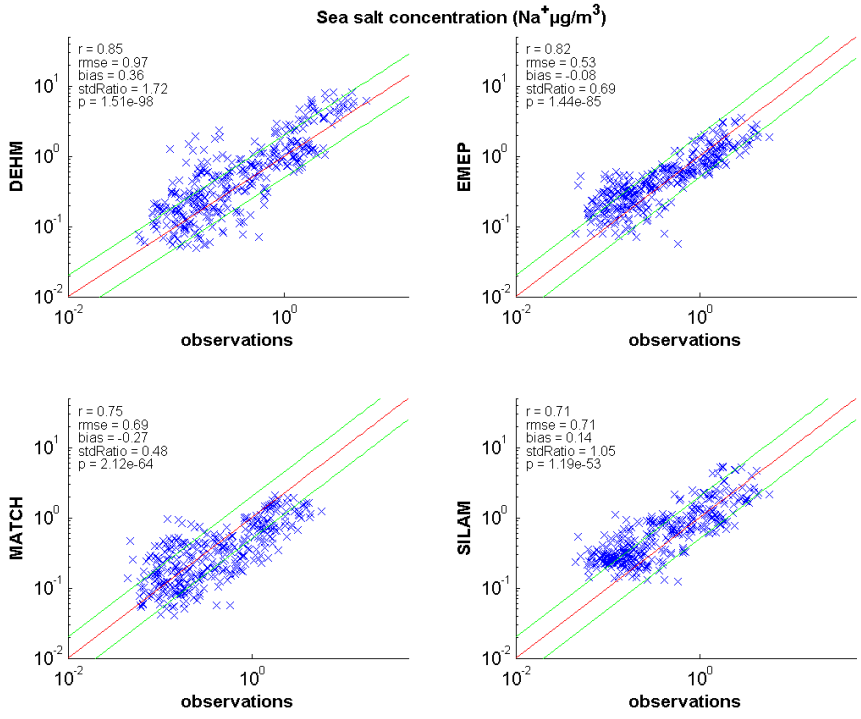

Figure 2. Model-measurement comparison for Na^+ monthly mean concentration (µg m^{-3}) for 29 EMEP measuring sites, between 1990 and 2009. The Person correlation (r), root mean square error (rmse), bias, standard deviation ration (stdRatio), p-value (p), 1:1 (red solid), 1:2 (green), and 2:1 (green) lines are shown for each CTM.

Atmos. Chem. Phys. Discuss., doi:10.5194/acp-2015-1056, 2016
Manuscript under review for journal Atmos. Chem. Phys.
Published: 16 February 2016

Atmospheric Chemistry and Physics Discussions

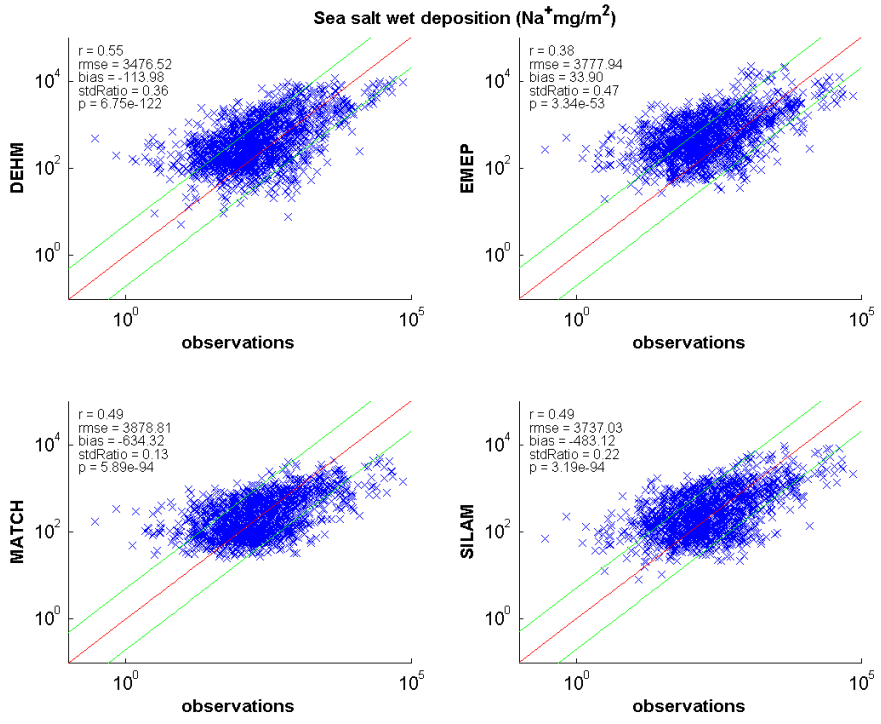

Figure 3. Model-measurement comparison for Na^+ monthly wet deposition (µg m^{-2}) for 133 EMEP measuring sites, between 1990 and 2009. The Person correlation (r), root mean square error (rmse), bias, standard deviation ration (stdRatio), p-value (p), 1:1 (red solid), 1:5 (green), and 5:1 (green) lines are shown for each CTM.

Atmos. Chem. Phys. Discuss., doi:10.5194/acp-2015-1056, 2016
Manuscript under review for journal Atmos. Chem. Phys.
Published: 16 February 2016

1

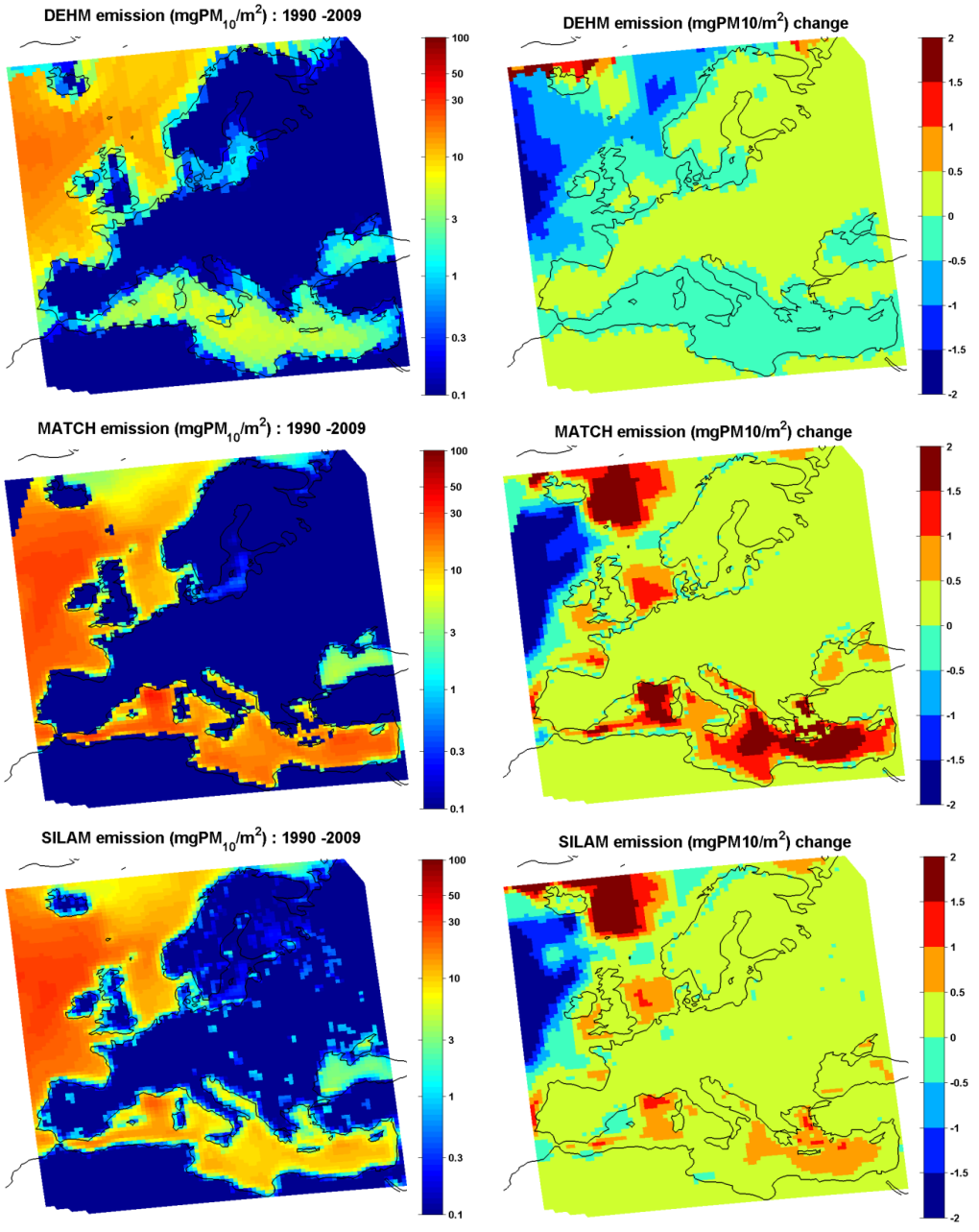

2 **Figure 4.** Annual sea salt emission ($mgPM_{10}\ m^{-2}$) for DEHM, MATCH and SILAM models.
3 Left panel mean value for the past period (1990-2009); right panel: absolute difference
4 between the future (2040-2059) and past periods.

Atmos. Chem. Phys. Discuss., doi:10.5194/acp-2015-1056, 2016
Manuscript under review for journal Atmos. Chem. Phys.
Published: 16 February 2016

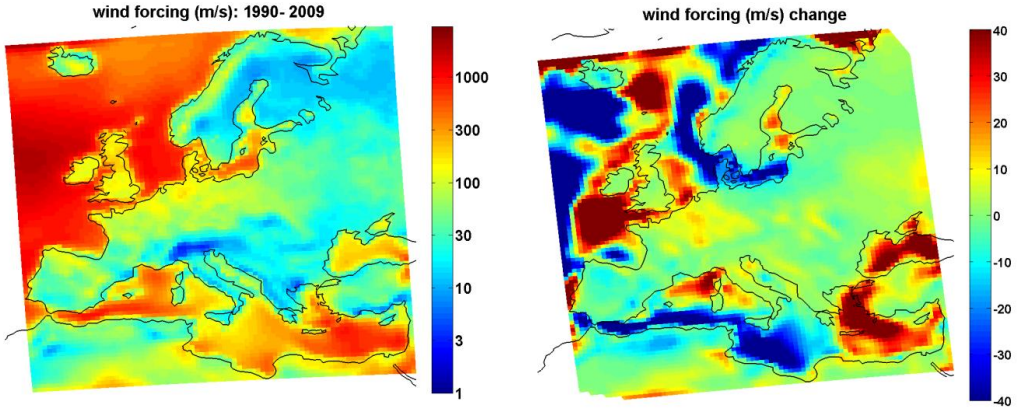

Figure 5. Wind forcing ($\approx U_{10}^{3.41}$). Left panel: past period (1990-2009); right panel: absolute difference between the future (2040-2059) and past periods.

Atmos. Chem. Phys. Discuss., doi:10.5194/acp-2015-1056, 2016
Manuscript under review for journal Atmos. Chem. Phys.
Published: 16 February 2016

1

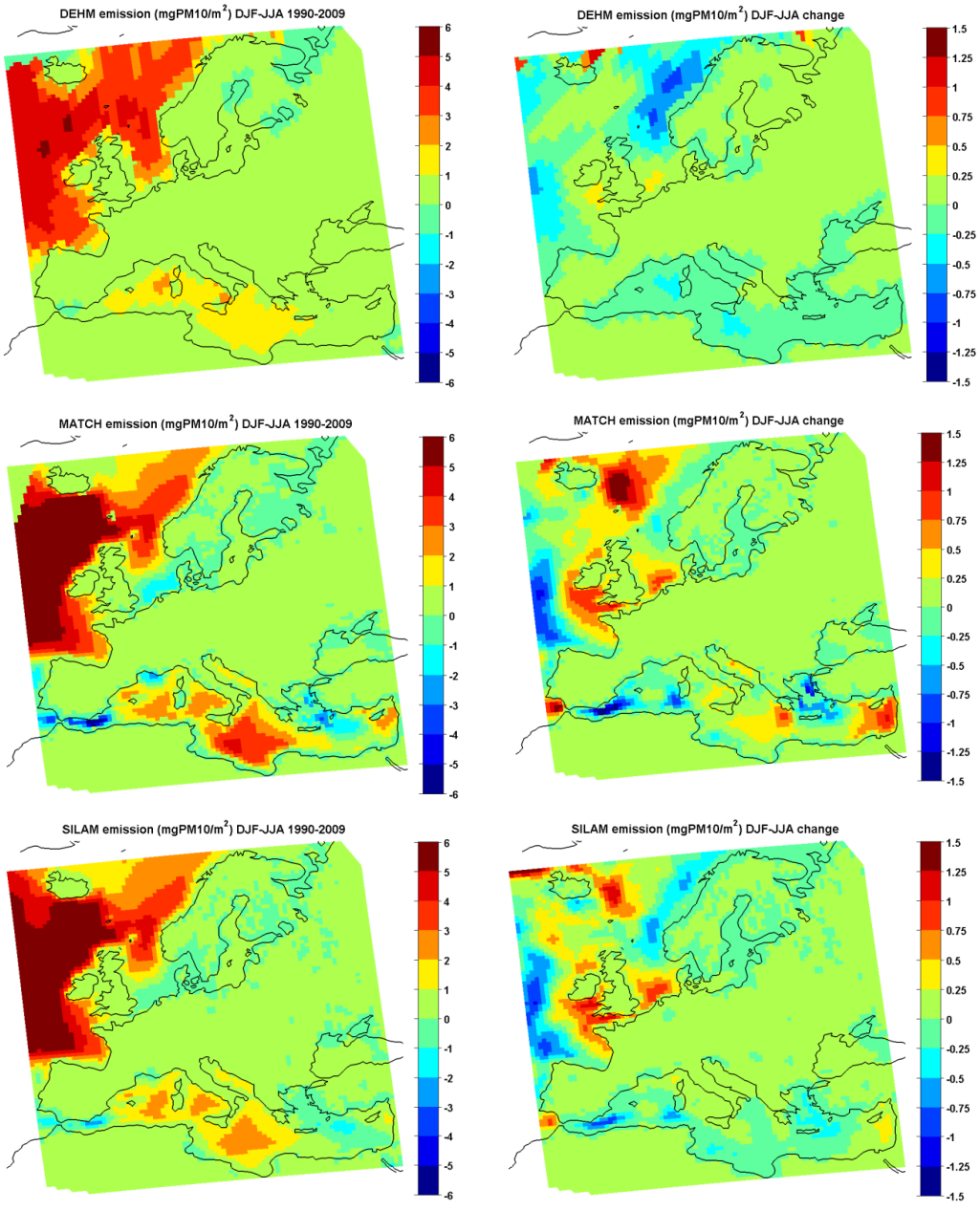

2 **Figure 6** Sea salt emission ($mgPM_{10}$ m^{-2}) difference between winter (December, January and
3 February, DJF) and summer (June, July and August, JJA) for DEHM, MATCH and SILAM

Atmos. Chem. Phys. Discuss., doi:10.5194/acp-2015-1056, 2016
Manuscript under review for journal Atmos. Chem. Phys.
Published: 16 February 2016

Atmospheric Chemistry and Physics Discussions

models. Left panel: past period (1990-2009); right panel: absolute difference between the future (2040-2059) and past periods.

Atmos. Chem. Phys. Discuss., doi:10.5194/acp-2015-1056, 2016
Manuscript under review for journal Atmos. Chem. Phys.
Published: 16 February 2016

Atmospheric Chemistry and Physics Discussions

1

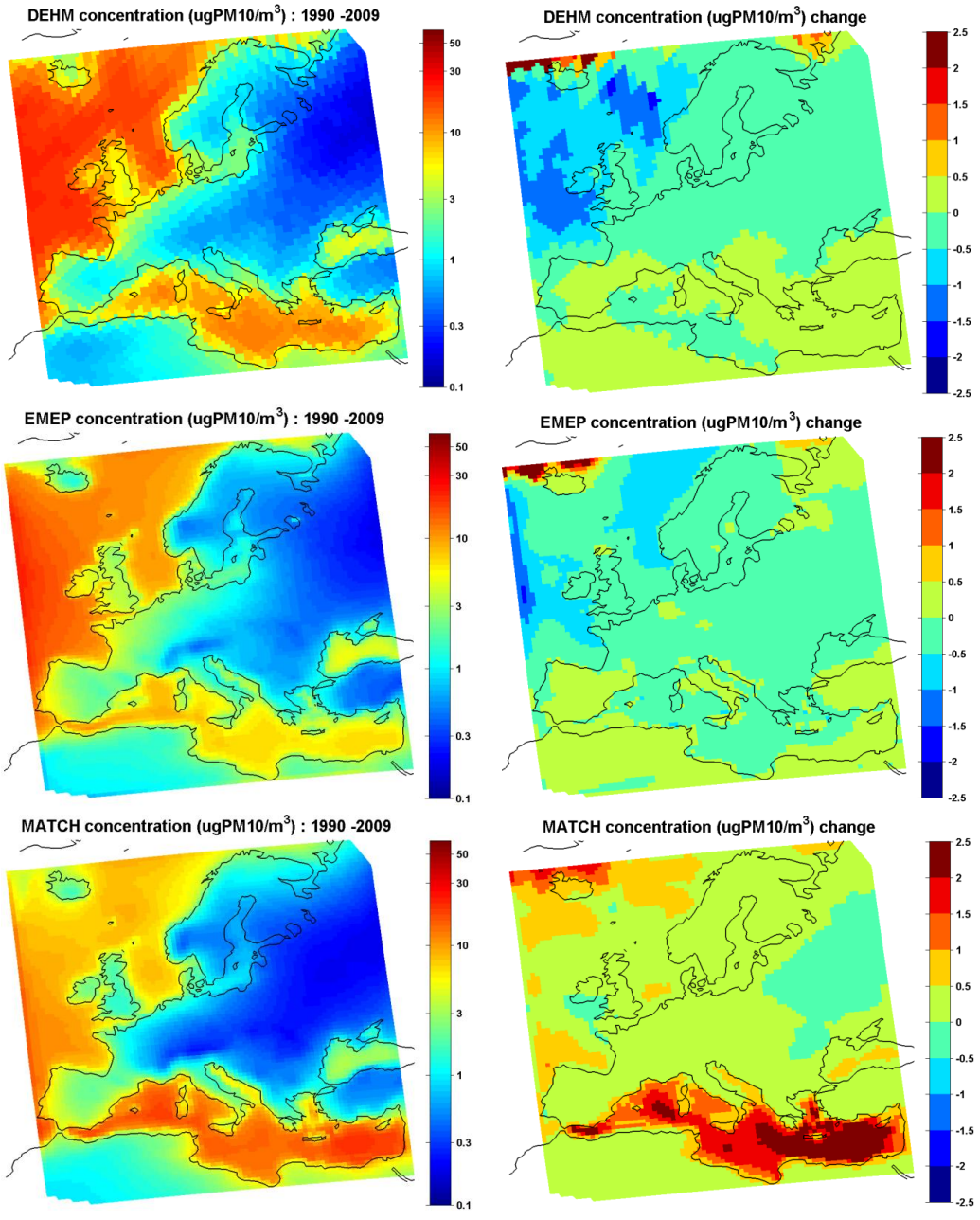

Atmos. Chem. Phys. Discuss., doi:10.5194/acp-2015-1056, 2016
Manuscript under review for journal Atmos. Chem. Phys.
Published: 16 February 2016

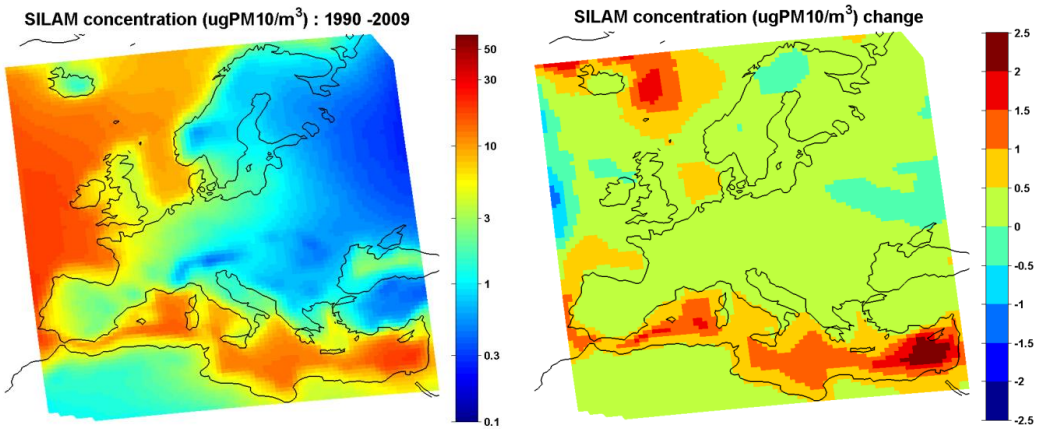

1

2 **Figure 7**. Sea salt surface concentration ($\mu gPM_{10}\ m^{-3}$) for DEHM, MATCH, EMEP and
3 SILAM models. Left panel: mean value for the past period (1990-2009); right panel: absolute
4 difference between the future (2040-2059) and past periods.

5

Atmos. Chem. Phys. Discuss., doi:10.5194/acp-2015-1056, 2016
Manuscript under review for journal Atmos. Chem. Phys.
Published: 16 February 2016

Atmospheric Chemistry and Physics Discussions

1

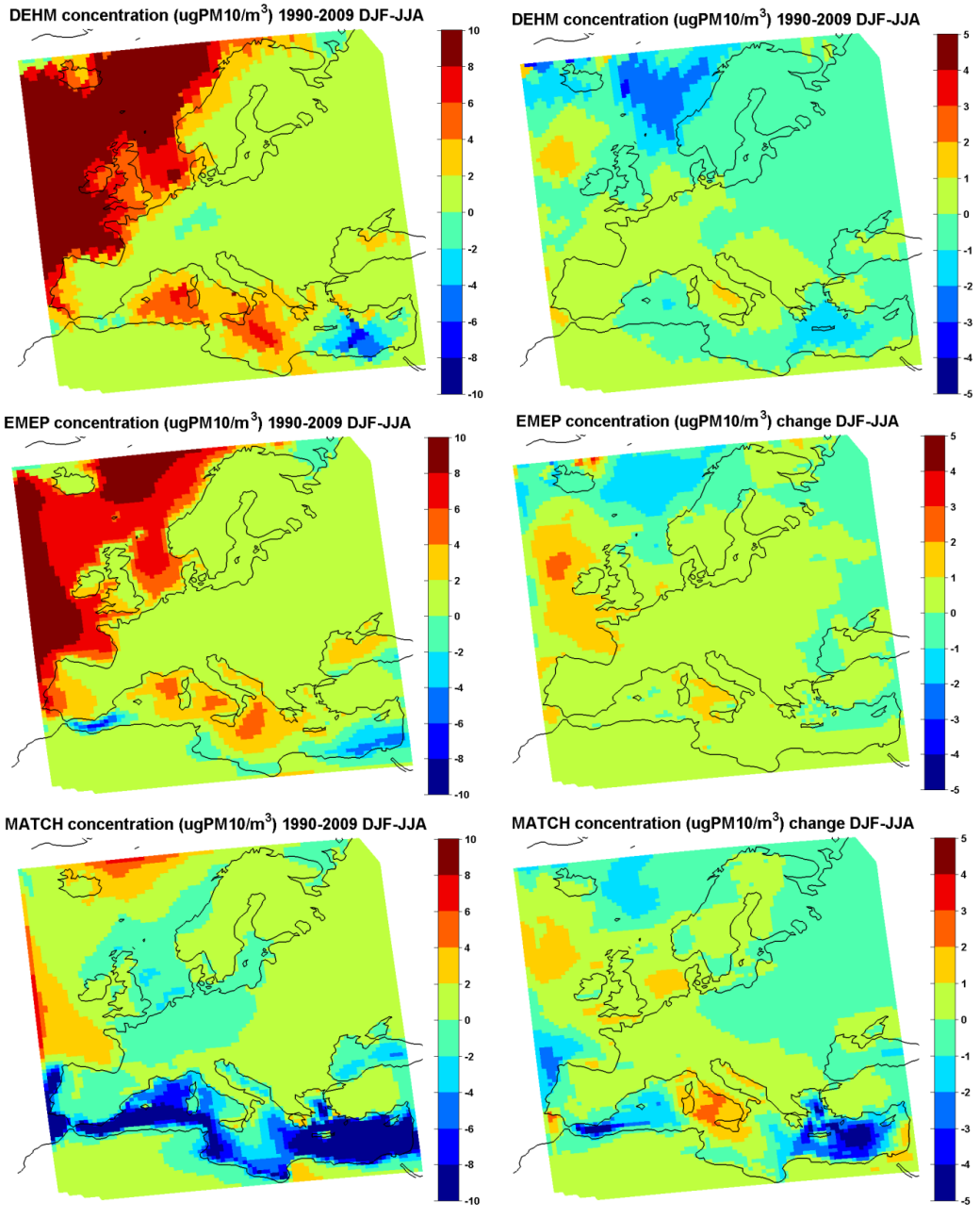

Atmos. Chem. Phys. Discuss., doi:10.5194/acp-2015-1056, 2016
Manuscript under review for journal Atmos. Chem. Phys.
Published: 16 February 2016

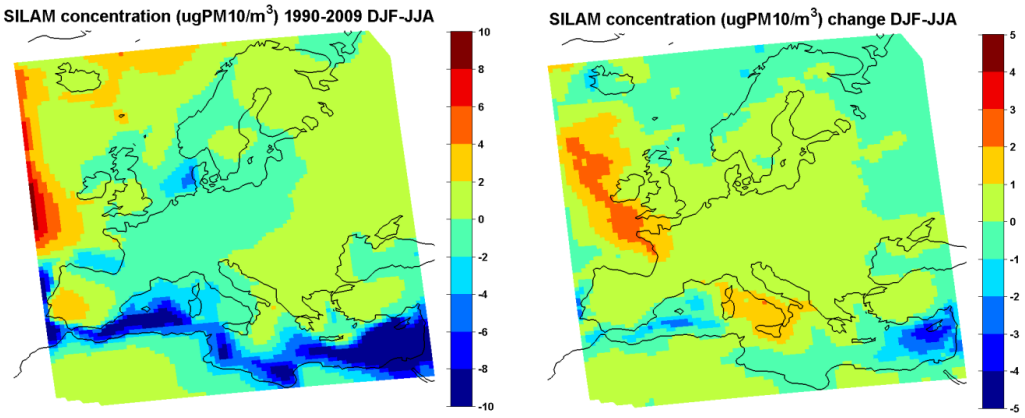

1

2 **Figure 8** Sea salt concentration ($\mu gPM_{10}\ m^{-3}$) difference between winter (December, January
3 and February, DJF) and summer (June, July and August, JJA) for DEHM, MATCH and
4 SILAM models. Left panel: past period (1990-2009); right panel: absolute difference between
5 the future (2040-2059) and past periods.

6

Atmos. Chem. Phys. Discuss., doi:10.5194/acp-2015-1056, 2016
Manuscript under review for journal Atmos. Chem. Phys.
Published: 16 February 2016

Atmospheric Chemistry and Physics Discussions

1

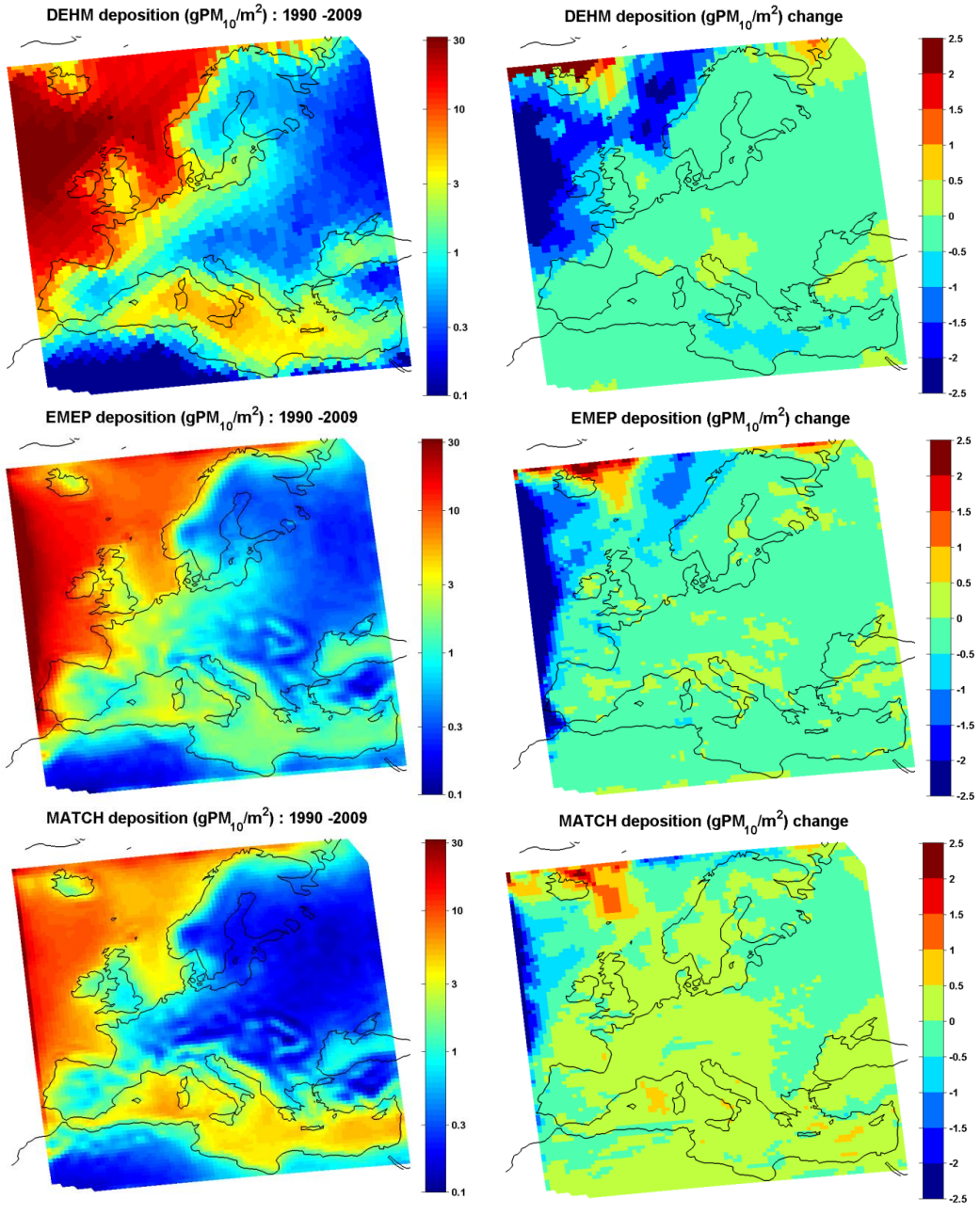

Atmos. Chem. Phys. Discuss., doi:10.5194/acp-2015-1056, 2016
Manuscript under review for journal Atmos. Chem. Phys.
Published: 16 February 2016

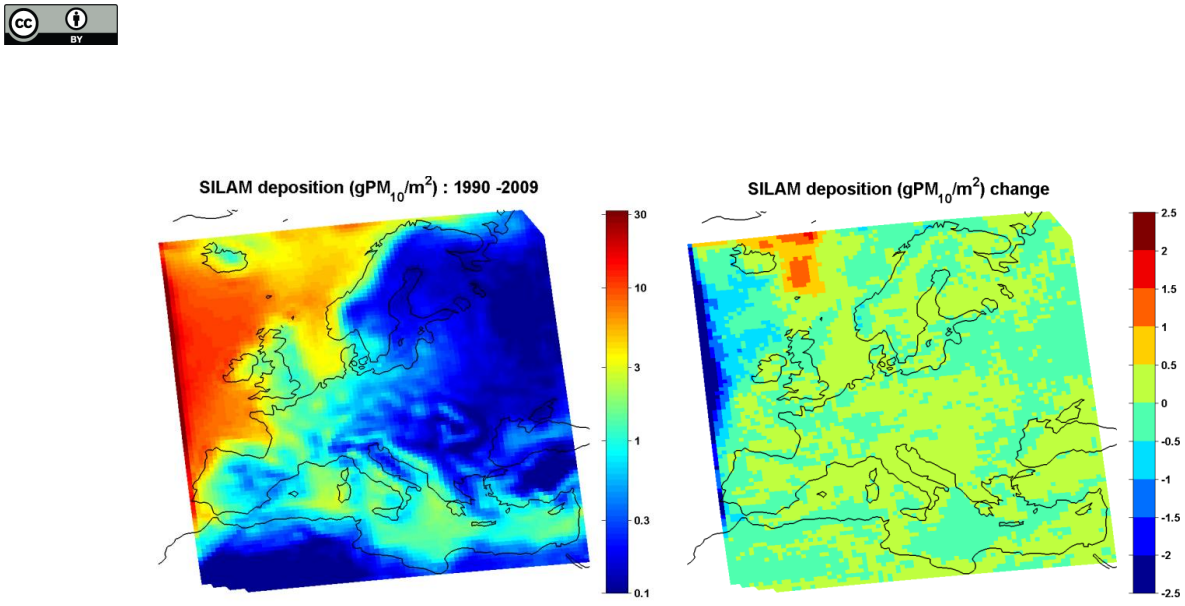

Figure 9 Sea salt deposition (wet+dry) ($mgPM_{10}$ m^{-2}) for DEHM, MATCH, EMEP and SILAM models. Left panel: mean value for the past period (1990-2009); right panel: absolute difference between the future (2040-2059) and past periods.

Atmos. Chem. Phys. Discuss., doi:10.5194/acp-2015-1056, 2016
Manuscript under review for journal Atmos. Chem. Phys.
Published: 16 February 2016

Atmospheric Chemistry and Physics Discussions

1

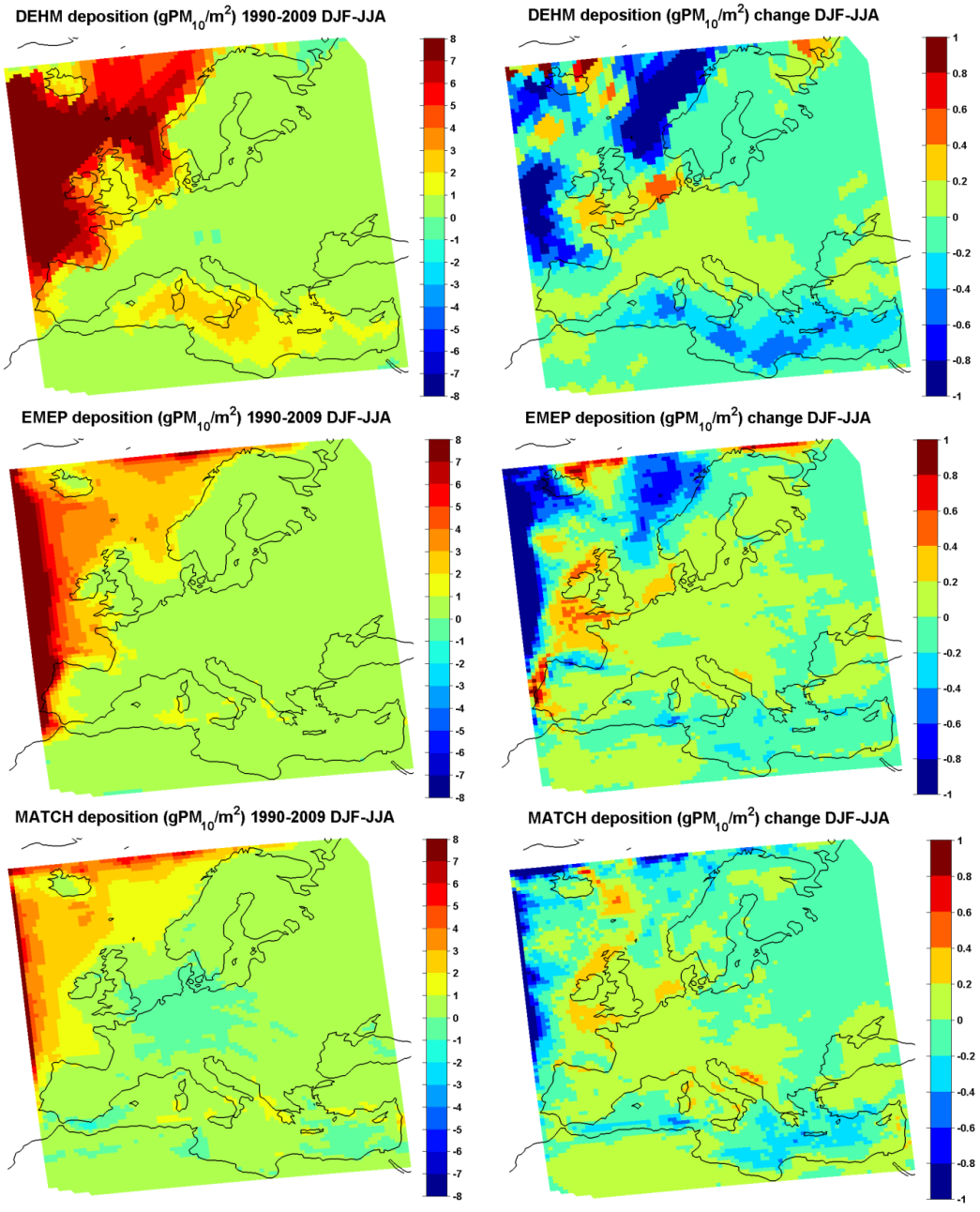

Atmos. Chem. Phys. Discuss., doi:10.5194/acp-2015-1056, 2016
Manuscript under review for journal Atmos. Chem. Phys.
Published: 16 February 2016

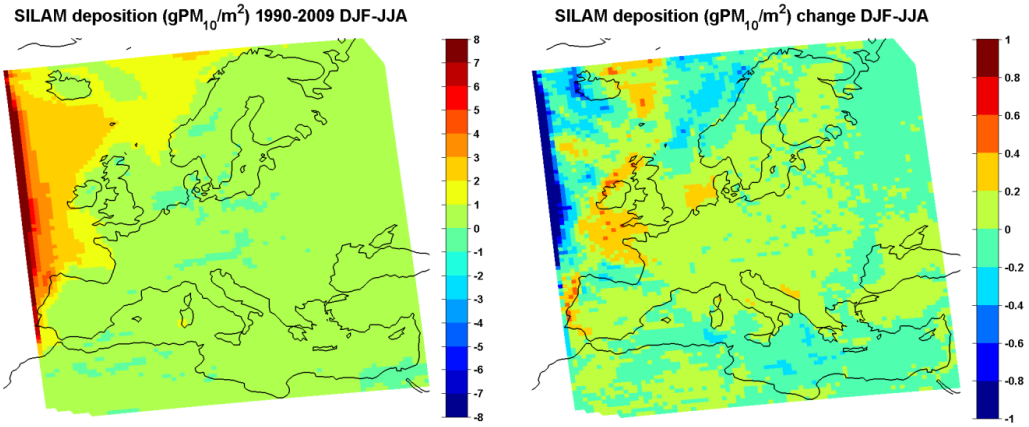

Figure 10 Sea salt annual deposition (gPM_{10} m^{-2}) difference between winter (December, January and February, DJF) and summer (June, July and August, JJA) for DEHM, MATCH and SILAM models. Left panel: past period (1990-2009); right panel: absolute difference between future (2040-2059) and past periods.

Atmos. Chem. Phys. Discuss., doi:10.5194/acp-2015-1056, 2016
Manuscript under review for journal Atmos. Chem. Phys.
Published: 16 February 2016

1

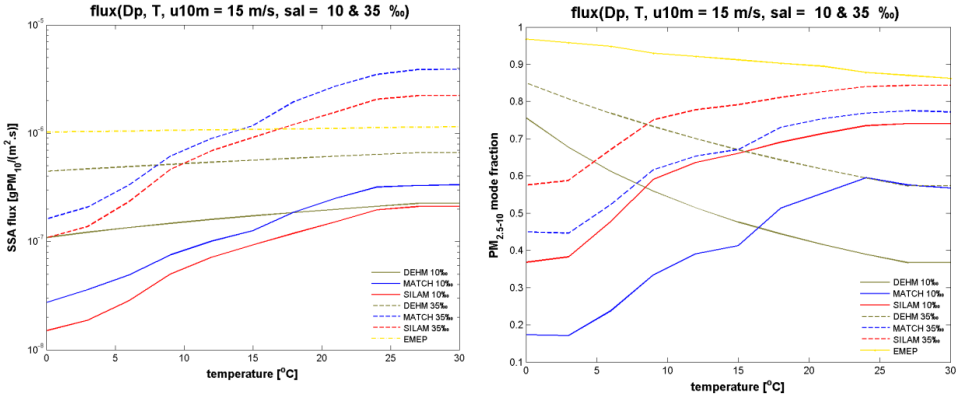

2

3 **Figure 11.** SSA mass flux [$gPM_{10}\ m^{-2}\ s^{-1}$)] box calculations (left) and coarse mode fraction of
4 the mass flux (right): as a function of radius (dry for DEHM and SILAM and RH = 80 % for
5 MATCH) and temperature, for wind speed 15 m s^{-1} and salinities 10 ‰ and 35 ‰.

6

Atmos. Chem. Phys. Discuss., doi:10.5194/acp-2015-1056, 2016
Manuscript under review for journal Atmos. Chem. Phys.
Published: 16 February 2016

1

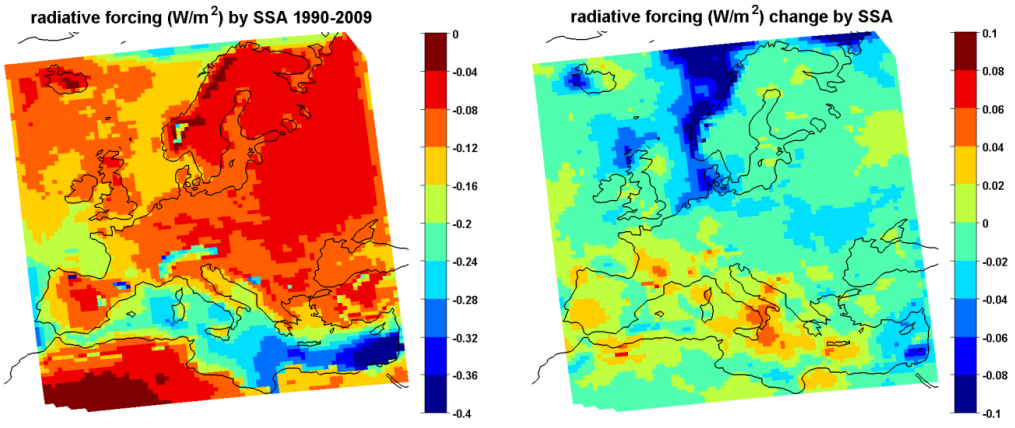

2

3 Figure 12. Radiative forcing by sea salt (W m^{-2}). Left panel: past period (1990-2009); right
4 panel: absolute difference between future (2040-2059) and past periods.

5

Atmos. Chem. Phys. Discuss., doi:10.5194/acp-2015-1056, 2016
Manuscript under review for journal Atmos. Chem. Phys.
Published: 16 February 2016

1

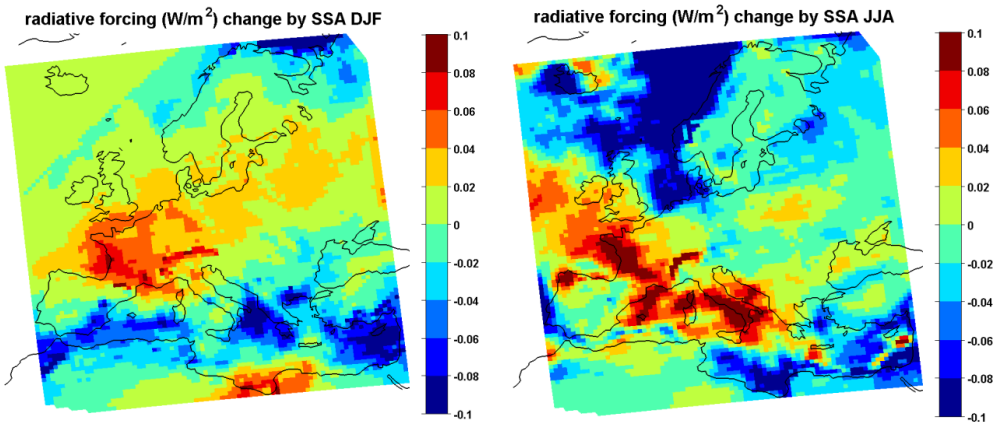

2

3 Figure 13. Radiative forcing by sea salt (W m^{-2}): difference between future (2040-2059) and
4 past periods. Left panel: winter (December, January and February); right panel: summer
5 (June, July and August)

6

7